Article

Cell Reports

CD109 Restrains Activation of Cutaneous IL-17-Producing γδ T Cells by Commensal Microbiota

Graphical Abstract

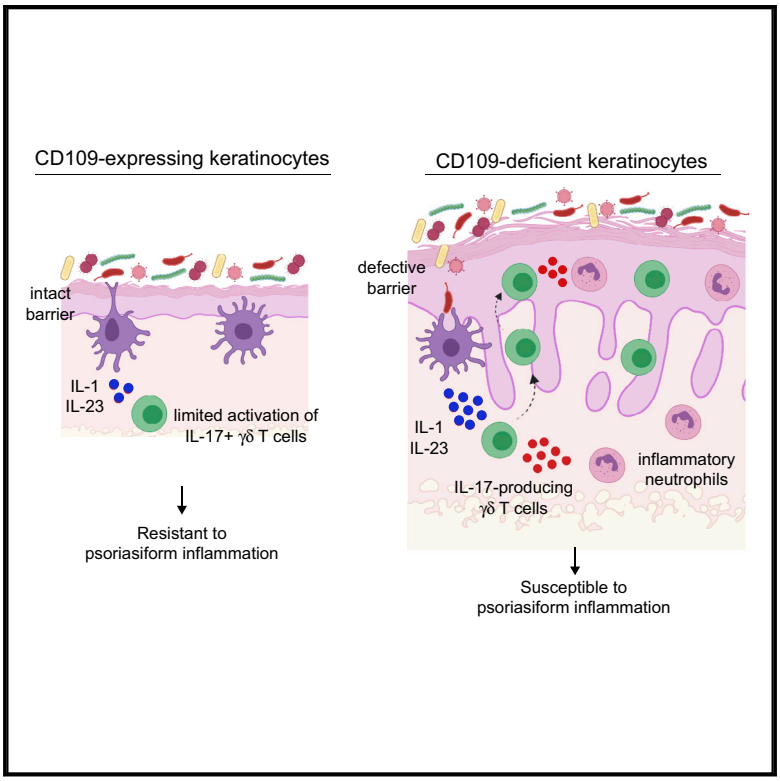

Authors

Hualin Zhang, Giustino Carnevale, Barbara Polese, ..., Donald C. Vinh, Roxane Pouliot, Irah L. King

Correspondence

irah.king@mcgill.ca

In Brief

Zhang et al. demonstrate that CD109 acts in a skin-specific and cell-extrinsic manner to regulate interleukin (IL)-17 production by cutaneous γδ T cells. Genetic loss of CD109 results in spontaneous skin inflammation and an enhanced susceptibility to psoriasiform inflammation, a phenotype that can be reversed with topical application of antibiotics.

Highlights

- CD109 is a negative regulator of the cutaneous IL-23/IL-17 immune axis
- Deletion of CD109 amplifies IL-17 production by skin γδ T cells
- CD109 enforces skin barrier integrity and reactivity to commensal microbiota

Zhang et al., 2019, Cell Reports *29*, 391–405
October 8, 2019
https://doi.org/10.1016/j.celrep.2019.09.003

CellPress

Cell Reports
Article

CD109 Restrains Activation of Cutaneous IL-17-Producing γδ T Cells by Commensal Microbiota

Hualin Zhang,[1,7] Giustino Carnevale,[1,6,7] Barbara Polese,[1] Melissa Simard,[5] Bavanitha Thurairajah,[1] Nargis Khan,[2] Maria E. Gentile,[1] Ghislaine Fontes,[1] Donald C. Vinh,[3,4] Roxane Pouliot,[5] and Irah L. King[1,2,8,*]

[1]Meakins-Christie Laboratories, Department of Microbiology and Immunology, McGill University Health Centre Research Institute, Montreal, QC, Canada
[2]Meakins-Christie Laboratories, Department of Medicine, McGill University Health Centre Research Institute, Montreal, QC, Canada
[3]Infectious Disease Susceptibility Program, McGill University Health Centre (MUHC) and Research Institute-MUHC (RI-MUHC), Montréal, QC, Canada
[4]Department of Human Genetics, McGill University, Montréal, QC, Canada
[5]CHU de Québec–Université Laval, Hôpital de l'Enfant-Jésus, Québec, QC, Canada
[6]Present address: Engene, Inc., 7171 Frederick-Banting, Montréal, QC H4S 1Z9, Canada
[7]These authors contributed equally
[8]Lead Contact
*Correspondence: irah.king@mcgill.ca
https://doi.org/10.1016/j.celrep.2019.09.003

SUMMARY

Interleukin-17-producing γδ T (γδ17) cells play a central role in protective and pathogenic immune responses. However, the tissue-specific mechanisms that control the activation of these innate lymphocytes are not known. Here, we demonstrate that CD109, a glycosylphosphatidylinositol (GPI)-anchored protein highly expressed by keratinocytes, is an important regulator of skin homeostasis and γδ17 cell activation. Genetic deletion of CD109 results in spontaneous epidermal hyperplasia, aberrant accumulation of dermal-derived γδ17 cells, and enhanced susceptibility to psoriasiform inflammation. In this context, γδ17 activation requires interleukin (IL)-23 signals and is reversed by transient depletion of the skin microbiota. Mechanistically, CD109 restrains γδ17 cell activation in a cell-extrinsic manner by fortifying skin barrier integrity. Collectively, our data provide insight into the regulation of the skin IL-23/IL-17 immune axis and how homeostasis is maintained at this important barrier site.

INTRODUCTION

Mammalian skin is a multi-layered barrier organ indispensable for host protection from environmental insults and invasion by pathogenic microorganisms. The outermost layer of the skin, the epidermis, is predominantly composed of a stratified epithelial cell network maintained by a single layer of self-renewing basal progenitor cells (Fuchs and Nowak, 2008). The underlying dermal tissue harbors a diverse leukocyte compartment that, upon epidermal barrier disruption or infection, is positioned to rapidly respond to injury or infection (Becher and Pantelyushin, 2012). Recently, a subset of innate-like γδ T lymphocytes has been described to seed the dermis within the first days of life and exhibit a self-renewal capacity (Cai et al., 2011; Gray et al., 2011; Sumaria et al., 2011). Dermal γδ T cells express a limited, but polyclonal, T cell receptor (TCR) repertoire enriched for Vγ4 usage and are imprinted in the thymus to express the lineage-specific transcription factor Rorγt, endowing them with the ability to produce interleukin (IL)-17-producing γδ T cells (referred to hereafter as γδ17 cells) (Ribot et al., 2009). Once resident in the skin, γδ17 cells can be activated upon exposure to inflammatory cytokines, such as IL-1 and IL-23, in a TCR-independent manner (Sutton et al., 2009). Their unique localization and effector functions make γδ17 cells important for early resistance against cutaneous pathogens such as *Staphylococcus aureus* and *Candida albicans* (Cho et al., 2010; Kashem et al., 2015). In these settings, IL-17 stimulates keratinocytes to produce anti-microbial factors and chemokines that recruit microbicidal neutrophils that together limit microbial dissemination (Becher and Pantelyushin, 2012). Although controversial, γδ17 cells have also been implicated in the chronic inflammatory disease psoriasis. Indeed, imiquimod-driven psoriasiform inflammation—characterized by epidermal hyperplasia and parakeratosis—in mice requires Vγ4$^+$ γδ17 cells (Gray et al., 2013), and two independent studies of human psoriatic disease identified increased numbers of γδ17 cells in lesioned skin compared to non-lesioned patient skin (Cai et al., 2011; Laggner et al., 2011). Thus, γδ17 cells must be tightly controlled to protect against pathogen invasion and prevent dysregulated responses that lead to chronic inflammation and disease.

The anatomical niche of cutaneous γδ17 cells positions them to be influenced by commensal microbial communities (i.e., the microbiota) on or within the skin barrier. For example, germ-free mice contain decreased numbers of dermal γδ17 cells compared to specific pathogen-free (SPF) mice (Naik et al., 2012). Conversely, the colonization of mice with commensal bacteria including *Corynebacterium* and *Staphylococcus* species results

in the non-inflammatory accumulation of γδ17 cells (Ridaura et al., 2018). In this context as well as in overt inflammatory conditions, IL-23 signaling is necessary for γδ17 cell cytokine production (Kashem et al., 2015). The IL-23/IL-17 immune axis is known to be triggered when injury- or infection-induced epithelial damage and barrier disruption exposes dermal mononuclear phagocytes to microbial-derived TLR ligands that initiate the activation of innate tissue-resident cell types (Gaffen et al., 2014). However, keratinocytes actively maintain a physical and chemical barrier that limits the exposure of leukocytes to commensal or pathogenic microbes. Currently, the mechanisms that control the activation of the cutaneous IL-23/IL-17 immune axis in general—and dermal γδ17 cells, specifically—to the commensal microbiota and other inflammatory stimuli are not clearly defined. Moreover, the diverse roles of this axis in the skin versus other barrier tissues, such as the intestine—where γδ17 cells promote barrier integrity (Lee et al., 2015)—provide the impetus for identifying tissue-specific mechanisms of immune regulation that may be harnessed to design therapies targeted to enhance barrier integrity while alleviating the pathology associated with psoriasis and other immune-mediated skin disorders.

CD109 is a glycosylphosphatidylinositol (GPI)-anchored membrane protein highly expressed in healthy skin and malignant tumor cells such as lung adenocarcinoma (Chuang et al., 2017; Mii et al., 2012). Mice lacking CD109 exhibit a delay in hair development, persistent epidermal hyperplasia, and high bone turnover (Mii et al., 2018, 2012). However, the specific impact of CD109 on the cutaneous immune system has not been examined. Here, we report CD109 as a selective regulator of the skin IL-23/IL-17 immune axis and γδ17 cells. A deficiency of CD109 in mice resulted in spontaneous inflammation of the skin, including epidermal hyperproliferation and thickening, neutrophil accumulation, and aberrant IL-23-dependent activation of dermal γδ17 cells. Consistent with a dysregulated IL-23/IL-17 pathway, the absence of CD109 led to enhanced psoriasiform inflammation following imiquimod application. We also demonstrate that CD109 acts in a skin-specific and cell-extrinsic manner to limit IL-23-dependent γδ17 activation by the commensal microbiota. Collectively, our data reveal CD109 as a negative regulator of host-microbiota crosstalk that restricts the activation of the cutaneous IL-23/IL-17 immune axis.

RESULTS

Deletion of CD109 Results in Spontaneous Skin Inflammation

Genetic deletion of CD109 in mice results in delayed hair growth that reaches normal density by 6–8 weeks of age (Mii et al., 2012). In addition, we observed that at 10–12 weeks of age, *CD109*$^{-/-}$ mice began to exhibit patchy hair loss that increased in area with age (Figure 1A). Consistently, we found CD109 to be highly expressed in the skin, but undetectable in lymph node cells and circulating leukocytes of wild-type (WT) animals (Figure 1B). Tissues from *CD109*$^{-/-}$ mice were used as negative controls (Figure 1B). In addition, markers of inflammation (e.g., *S100a8* and *S100a9*) (Kerkhoff et al., 2012) increased with age in the skin of *CD109*$^{-/-}$ mice, coupled with significant ear thickening and epidermal hyperplasia by 10 weeks of age (Figures 1C–1F). These results prompted us to examine the skin tissue of *CD109*$^{-/-}$ mice in greater detail. Epidermal hyperplasia in 8- to 12-week-old *CD109*$^{-/-}$ mice was associated with an increase in the presence of epidermal and dermal cell proliferation, as determined by Ki67 expression using immunofluorescence microscopy and *ex vivo* flow cytometry analysis in hematopoietic (*CD45*$^{+}$) and non-hematopoietic (*CD45*$^{-}$) compartments (Figure 1G and 1H). Increased cell proliferation was associated with inflammation, as ears from *CD109*$^{-/-}$ mice contained Ly6G+ neutrophils in both epidermal and dermal layers that were essentially absent in WT controls (Figures 1G, 1I, and IJ). These results indicate that a loss of CD109 results in spontaneous and progressive skin inflammation.

Dysregulation of the Cutaneous IL-23/IL-17 Immune Axis in the Absence of CD109

To determine the immune pathways associated with the observed spontaneous skin inflammation in *CD109*$^{-/-}$ mice, we extracted total RNA from epidermal and dermal layers of ears from WT and *CD109*$^{-/-}$ mice and performed targeted gene expression analysis using Nanostring technology. Transcript analysis indicated a significant increase in cytokine gene expression in skin from *CD109*$^{-/-}$ compared to WT controls associated with the IL-23/IL-17 immune axis, including *Il17a*, *Il17f*, *Il19*, *Il20*, *Il22*, and *Il23a* (Figure 2A). qRT-PCR analysis of selected transcripts confirmed a significant increase in *Il17a* expression from *CD109*$^{-/-}$ skin, but no significant differences in cytokine mRNA characteristic of type 1 or type 2 immunity—such as *Ifng* or *Il4* or *Il5*, respectively—with the exception of *Il13* that was decreased in the epidermis of *CD109*$^{-/-}$ mice compared to controls (Figures 2B and 2C). Consistent with these data, spontaneous secretion of IL-17A, but not IFNγ or IL-13, was detected in cultures of total skin cells from *CD109*$^{-/-}$, but not WT, mice (Figure 2D). Furthermore, the deletion of IL-17-producing cells in *CD109*$^{-/-}$ mice by crossing these animals to Rorγt$^{GFP/GFP}$ mice in which GFP is knocked into the *Rorgt* locus, a transcription factor required for the differentiation of IL-17-producing cells (Ivanov et al., 2009), prevented epidermal hyperplasia in comparison to WT or *CD109*$^{-/-}$ *Rorγt*$^{GFP/+}$ controls (Figures 2E and 2F).

Previous studies indicate that CD109 negatively regulates canonical TGFβ signaling (Litvinov et al., 2011). However, we were unable to detect a difference in SMAD2/3 activation between WT and *CD109*$^{-/-}$ total skin cells *ex vivo* or following *in vitro* stimulation with recombinant TGFβ1 (Figure 2G). By contrast, and consistent with a previous report (Mii et al., 2012), we observed a spontaneous activation of STAT3 in adult and neonatal *CD109*$^{-/-}$ but not WT skin cells, a transcription factor downstream of numerous cytokines associated with the IL-23/IL-17 immune axis and keratinocyte dysregulation (Figures 2G and 2H) (Sano et al., 2005). Thus, the absence of CD109 results in the spontaneous and selective activation of the cutaneous IL-23/IL-17 immune axis.

As IL-17 can be produced by diverse immune cell types, we determined the source of this cytokine by flow cytometric analysis. As our gene expression analysis indicated an increased expression of *Il17a* and *Il17f* in both epidermal and dermal

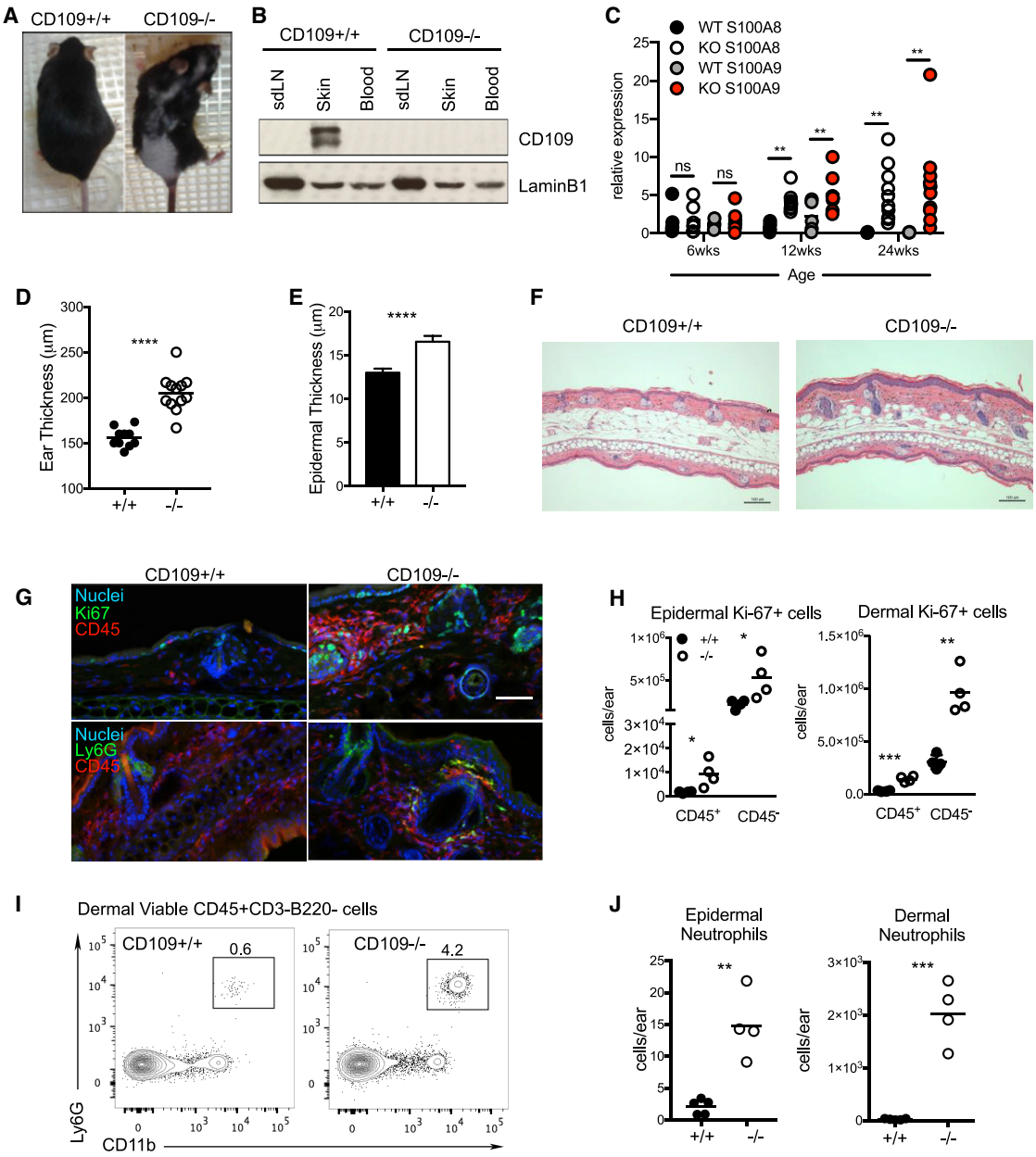

Figure 1. Spontaneous Skin Inflammation in *CD109*$^{-/-}$ Mice

(A) Phenotype of 12-week-old *CD109*$^{+/+}$ and *CD109*$^{-/-}$ mice.

(B) Immunoblot of CD109 expression in skin-draining lymph nodes, skin, and blood from CD109 and *CD109*$^{-/-}$ mice.

(C) qRT-PCR analysis of *S100a8* and *S100a9* expression in the skin of *CD109*$^{+/+}$ and *CD109*$^{-/-}$ mice at 6, 12, and 24 weeks of age.

(D and E) Quantification of ear (D) and epidermal (E) thickness.

(F) Hematoxylin and eosin staining of ear sections from *CD109*$^{+/+}$ and *CD109*$^{-/-}$ mice. Scale bars: 100 μm.

(G) Cross-section staining of *CD45*$^{+}$*Ki-67*$^{+}$ and *CD45*$^{+}$*Ly6G*$^{+}$ cells from *CD109*$^{+/+}$ and *CD109*$^{-/-}$ ears. Scale bars: 50 μm.

(H) Total cell counts of epidermal and dermal *CD45*$^{+}$*Ki-67*$^{+}$ and *CD45*$^{-}$*Ki-67*$^{+}$ cells in *CD109*$^{+/+}$ and *CD109*$^{-/-}$ mice.

(I) Representative contour plots of dermal neutrophils. Numbers indicate the frequency of *CD11b*$^{+}$*Ly6G*$^{+}$ cells from the viable *CD45*$^{+}$*CD3*$^{-}$*B220*$^{-}$ population.

(J) Cell counts of epidermal and dermal *CD11b*$^{+}$*Ly6G*$^{+}$ neutrophils.

In (A), (B), and (D)–(J), data are representative of at least three independent experiments containing 4 mice per group between 8 and 12 weeks of age. Each circle in the graphs represents an individual mouse. Error bars represent standard deviation. Mann-Whitney test (C, H, and J) and Student's t test (D and E); *$p < 0.05$, **$p < 0.01$, ***$p < 0.001$, ****$p < 0.0001$.

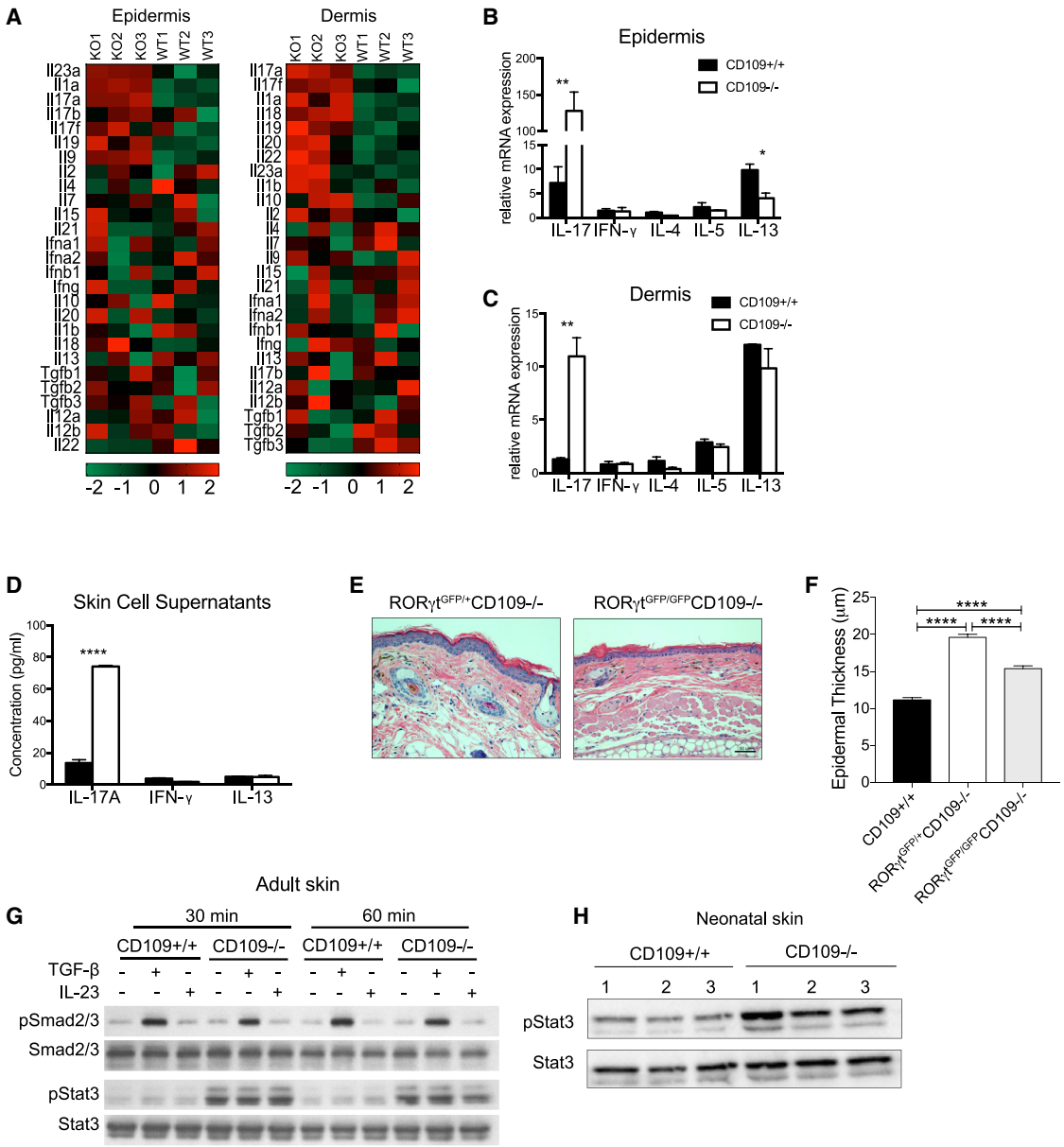

Figure 2. Loss of CD109 Activates the Cutaneous IL-23/IL-17 Immune Axis

(A) A heatmap of epidermal and dermal cytokine mRNA comparing *CD109*$^{+/+}$ (WT) and *CD109*$^{-/-}$ (KO) samples, with three samples of each genotype.

(B and C) qRT-PCR analysis for mRNA expression of epidermal (B) and dermal (C) cytokines.

(D) ELISA analysis of IL-17A, IFNγ, and IL-13 from supernatants of cultured *CD109*$^{+/+}$ and *CD109*$^{-/-}$ skin cells.

(E) Hematoxylin and eosin staining of ear sections from *RORγt*$^{GFP/+}$*CD109*$^{-/-}$ and RORγt$^{GFP/GFP}$*CD109*$^{-/-}$ mice. Scale bars: 50 μm.

(F) Quantification of epidermal thickness from the indicated groups.

(G) Immunoblot of phospho-Smad2/3, Smad2/3, phospho-Stat3, and Stat3 in the whole-skin lysates from skin cells in the context of TGF-β and IL-23 stimulation.

(H) Immunoblot of phospho-Stat3 and Stat3 in *ex vivo* whole-skin lysates from neonatal mice.

In (B)–(F), data are representative of three independent experiments containing 3 or 4 mice per group. Error bars represent standard deviation. Unpaired Student's t test; **p < 0.01, ****p < 0.0001.

skin layers of *CD109*$^{-/-}$ mice (Figure 2A), we analyzed each compartment separately. C57BL/6 mice contain a monoclonal population of epidermal-resident TCRδ^{hi}Vγ5^{+}δ1^{+} T cells (referred to as dendritic epidermal T cells [DETCs]) and a population of polyclonal dermal αβ and γδ T cells (Sumaria et al., 2011). As expected, CD45+ epidermal cells from WT mice were almost exclusively CD3^{hi}TCRδ^{hi} T cells (mean, 94.3%; SD, 1.3 from four representative mice), whereas the dermis contained TCRδ^{lo} and TCRδ^{-} cell subsets (Figures 3A and S1). Dermal cells from WT mice also contained a small

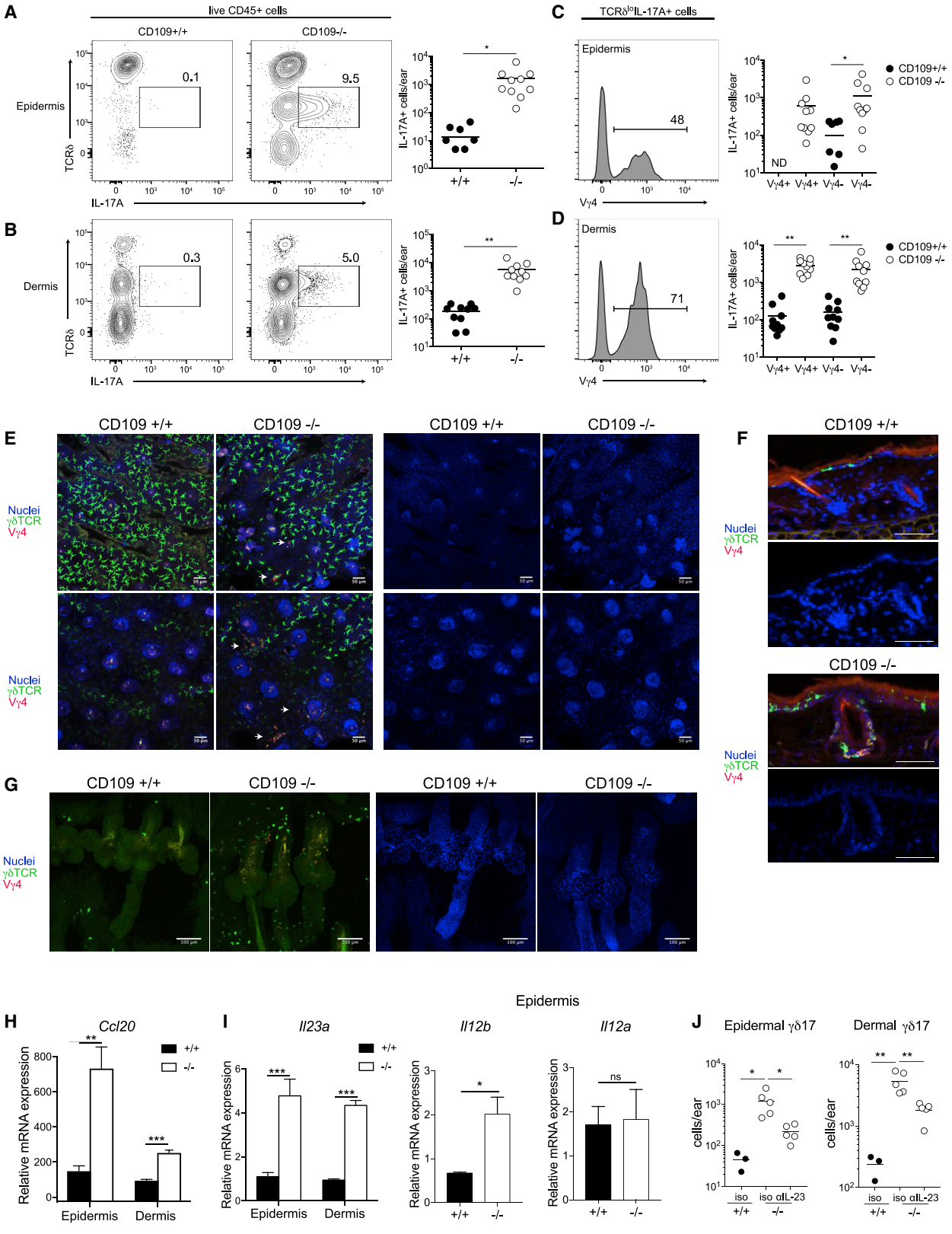

(legend on next page)

population of TCRδ^{hi} cells that were likely contaminating the DETCs (mean, 6.4%; SD, 2.7 from four representative mice) (Figure 3B). Consistent with previous reports, WT mice contained a population of dermal TCRδ^{lo} cells that produced IL-17A upon *in vitro* stimulation that was rare in epidermal preparations (Figures S1A–S1C) (Naik et al., 2012). By comparison, *CD109*$^{-/-}$ mice harbored a substantial population of γδ17 cells in the epidermis (Figures S1A–S1C). To determine whether γδ T cells were capable of producing IL-17 not only following *in vitro* stimulation, but also *in vivo*, we assessed the spontaneous production of IL-17A by *ex vivo* antibody labeling. While spontaneous IL-17 production was not detectable in WT skin cells, spontaneous IL-17A production was observed in both epidermal and dermal cells from *CD109*$^{-/-}$ skin and was limited to the TCRδ^{lo} compartment, indicating that these were dermal-derived γδ T cells (Figures 3A and 3B; see Figures S1D and S1E for further phenotyping). Next, we determined if the γδ17 cells in the skin of *CD109*$^{-/-}$ mice were selectively derived from the Vγ4^{+} lineage (Heilig and Tonegawa, 1986), a γδ T cell subset imprinted with IL-17-producing potential (Ribot et al., 2009). Indeed, a large percentage of epidermal and dermal γδ17 cells from *CD109*$^{-/-}$ mice expressed the Vγ4 T cell receptor subunit (Figures 3C and 3D). Although the dermal γδ T cell population also has been reported to include Vγ1^{+} and Vγ6^{+} subsets (Cai et al., 2014), we were unable to detect Vγ1^{+} cells in the skin of WT or *CD109*$^{-/-}$ mice from our animal colony despite their clear presence in the skin-draining lymph nodes (Figures S2A–S2C). As antibodies detecting the Vγ6 subset are not commercially available, we considered *Vγ4*$^{-}$*Vγ1*$^{-}$ γδ T cells as *Vγ6*$^{+}$ cells by exclusion. As shown in Figure S2B, a significant proportion of the *IL-17*$^{+}$ γδ T cell population was *Vγ4*$^{-}$*Vγ1*, suggesting that both Vγ4^{+} and Vγ6^{+} subsets of dermal γδ17 cells accumulate in the absence of CD109. Although all of our experiments comparing WT and *CD109*$^{-/-}$ mice were performed with mice initially reared from the same founder dams, environmental differences can occur following cage separation that may have impacted our results. To rule out this concern, we enumerated cutaneous γδ17 cells isolated from WT, *CD109*$^{+/-}$, and *CD109*$^{-/-}$ mice littermates raised in the same cage until sacrifice. Consistent with the results shown in Figure 3, *CD109*$^{-/-}$ mice still harbored significantly more epidermal and dermal γδ17 cells compared to the WT controls (Figures S3A and S3B). Interestingly, we did observe a gene dosage effect in that *CD109*$^{+/-}$ more closely resembled *CD109*$^{-/-}$ mice in terms of cutaneous γδ17 cell numbers (Figures S3A and S3B).

To confirm the epidermal localization of dermal-derived γδTCR^{+} cells, we performed confocal immunofluorescent microscopy of WT and *CD109*$^{-/-}$ skin (Figures 3E–3G). Whole-mount microscopy of epidermal sheets revealed the presence of TCRδ^{hi} DETCs extending processes across the more superficial layers of the epidermis in both WT and *CD109*$^{-/-}$ mice, as previously described (Figure 3E) (Nielsen et al., 2017). However, consistent with our flow cytometry analyses, clusters of rounded *Vγ4*$^{+}$ and *Vγ4*$^{-}$TCRδ^{lo} cells localized to the deeper layers of the epidermis of *CD109*$^{-/-}$, but not WT, skin (Figure 3E). Labeling of cross-sectioned skin samples confirmed the accumulation of Vγ4^{+} and Vγ4^{-}TCRδ^{lo} cells in the epidermis of *CD109*$^{-/-}$ mice, in close proximity to the hair follicle (Figure 3F). Finally, whole-mount microscopy of inverted epidermal sheets further demonstrated an increase of Vγ4^{+}TCRδ^{lo} clusters surrounding the hair follicle in *CD109*$^{-/-}$, but not WT, skin. (Figure 3G). Consistently, the neutrophils were also present within the *CD109*$^{-/-}$, but not WT, hair follicles (Figure S3C). These results coincided with an increase in mRNA expression of CCL20, a chemokine that promotes leukocyte migration to the hair follicle (Scharschmidt et al., 2017), in *CD109*$^{-/-}$ mice compared to controls (Figure 3H). Taken together, the absence of CD109 results in an accumulation of diverse dermal γδ17 cell subsets and their mislocalization to the epidermal layer of the skin.

An accumulation of γδ17 cells in both the epidermis and dermis of *CD109*$^{-/-}$ mice—as well as the increased expression of *Il23a* and *Il12b* (that encode for IL-23p19 and IL-12/23p40, respectively), but not *Il12a* (IL-12p35), mRNA in these tissues (Figure 3I and Nanostring analysis)—prompted us to determine the relevance of IL-23 in this setting, given that the production of IL-17 by γδ T cells can occur in both IL-23-dependent and IL-23-independent manners (Lee et al., 2015; Ridaura et al., 2018). To this end, we administered anti-IL-12/23p40 neutralizing antibodies or an isotype control to 10- to 12-week-old *CD109*$^{-/-}$ mice. Following 2 weeks of antibody treatment, the number of γδ17 cells was detected by flow cytometric analysis. Temporary anti-IL-12/23p40 blockade significantly decreased the number of γδ17 cells in both the epidermis and dermis to numbers approximating age-matched WT controls (Figure 3J). Thus, the spontaneous accumulation of cutaneous γδ17 cells requires IL-23 activity.

Figure 3. γδT Cells Accumulate in the Epidermis and Are the Dominant Source of IL-17A in *CD109*$^{-/-}$ Skin

(A and B) Contour plots of live *CD45*$^{+}$ epidermal (A) or dermal (B) cells showing the cellular source and frequency of IL-17A-producing cells (left) in *CD109*$^{+/+}$ and *CD109*$^{-/-}$ mice. Total cell counts of epidermal and dermal IL-17-producing cells (right).

(C and D) Histograms showing the frequency of *Vγ4*$^{+}$ cells within the IL-17A-producing TCRδ^{lo} cell population from the epidermis (C) and dermis (D) of *CD109*$^{-/-}$ mice (left). Total cell counts of epidermal and dermal IL-17-producing cells *Vγ4*$^{+}$ and *Vγ4*$^{-}$γδ T cells (right).

(E and F) Confocal microscopy images of whole-mount (E) and cross-section (F) staining for Vγ4, TCRδ, and nucleated cells in *CD109*$^{+/+}$ and *CD109*$^{-/-}$ ears. Arrows in (E) denote *Vγ4*$^{+}$*TCRδ*$^{+}$ cells. Scale bar: 50 μm.

(G) Confocal microscopy images of epidermal whole-mount staining for Vγ4 and TCRδ in *CD109*$^{+/+}$ and *CD109*$^{-/-}$ tail skin. Scale bar: 100 μm.

(H) *Ccl20* mRNA expression in epidermal and dermal sheets from ear skin of *CD109*$^{+/+}$ and *CD109*$^{-/-}$ mice.

(I) *Il23a*, *Il12a*, and *Il12b* mRNA expression in epidermal and dermal sheets from ear skin of *CD109*$^{+/+}$ and *CD109*$^{-/-}$ mice. Error bars indicate standard deviation.

(J) Total cell counts of epidermal and dermal γδ17 cells after 2 weeks of treatment with anti-IL-12/23p40 neutralizing antibody. Each circle represents an individual mouse.

(A–D) Pooled data from two independent experiments with 5 mice/group. (E and F) Representative images from at least 5 mice per genotype. (H and I) Representative data from three independent experiments containing 3 mice/group. (J) Representative data from three independent experiments with 3–5 mice/group. Unpaired Student's t test; *p < 0.05, **p < 0.01, ***p < 0.001. ns, not significant.

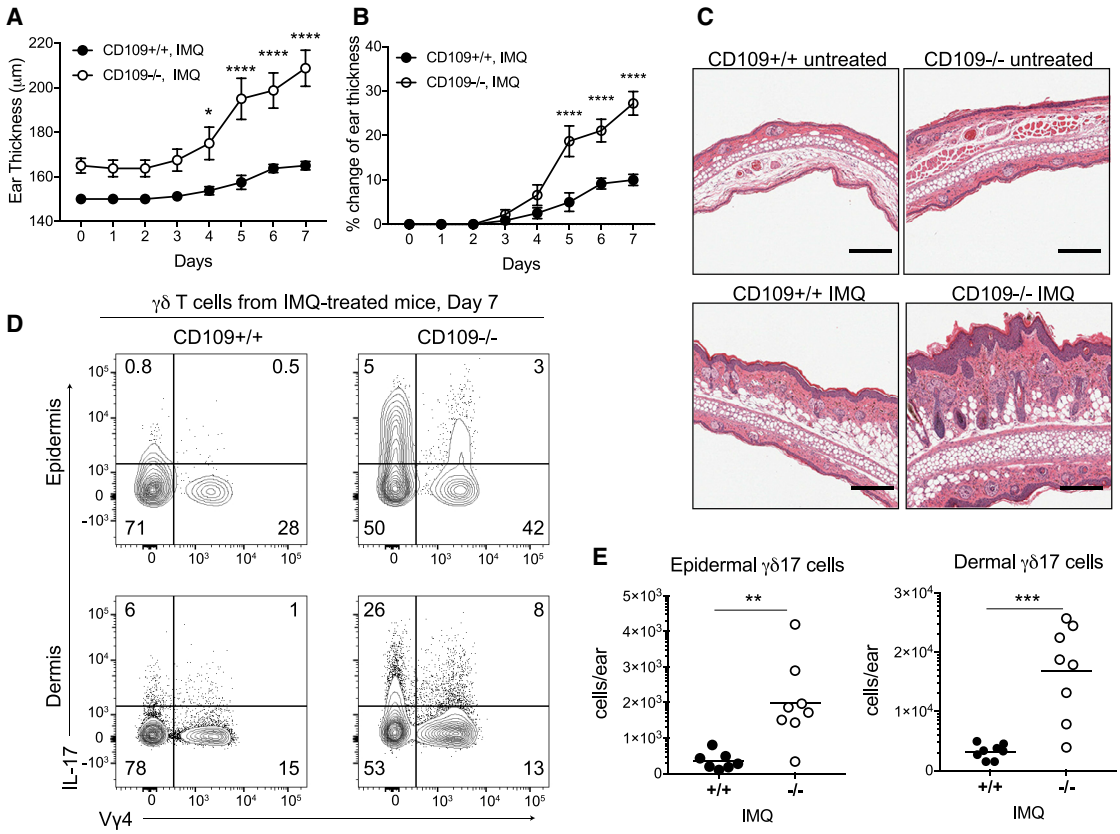

Figure 4. Loss of CD109 Enhances the Severity of Psoriasiform Inflammation

(A) Ear thickness measurements over 7 days of daily IMQ administration to *CD109*$^{+/+}$ and *CD109*$^{-/-}$ mice.

(B) Same data from (A) shown as a change in ear thickness relative to untreated controls from each genotype. Two-way ANOVA with multiple comparisons; *$p < 0.05$, ***$p < 0.001$.

(C) Representative H&E stained cross-sections from untreated or IMQ-treated ears from *CD109*$^{+/+}$ and *CD109*$^{-/-}$ mice.

(D) Representative contour plots of epidermal and dermal viable *CD45*$^{+}$*CD3*$^{+}$*B220*$^{-}$*TCRβ*$^{-}$*TCRδ*^{lo} population γδT cells. Numbers indicate the frequency of cells expressing Vγ4 and producing IL-17 without *ex vivo* stimulation.

(E) Total cell counts of epidermal and dermal γδ17 cells in *CD109*$^{+/+}$ and *CD109*$^{-/-}$ ears after 7 days of IMQ treatment. Each circle represents an individual mouse. Unpaired Student's t test; **$p < 0.01$ and ***$p < 0.001$. Data shown are pooled from two independent experiments with 4 mice/group. Scale bar: 200 μm.

CD109 Deficiency Enhances the Severity of Psoriasiform Inflammation

Dysregulation of the IL-23/IL-17 immune axis and STAT3 activation are associated with psoriasiform inflammation in both humans and mice (Cai et al., 2011; Sano et al., 2005). Given that *CD109*$^{-/-}$ mice exhibited a similar dysregulation of these pathways, and that decreased amounts of the CD109 protein have been found in lesioned compared to non-lesioned skin of individuals with psoriasis (Litvinov et al., 2011), we hypothesized that a loss of CD109 may predispose mice to a more severe form of psoriasiform inflammation. To this end, we treated the ear skin of *CD109*$^{+/+}$ and *CD109*$^{-/-}$ mice with low-dose imiquimod (IMQ; 3.75% w/v), a TLR7/8 agonist that triggers many of the clinical characteristics of psoriasis in an IL-23- and IL-17-dependent manner (van der Fits et al., 2009). Compared to the *CD109*$^{+/+}$ controls, *CD109*$^{-/-}$ mice exhibited a greater absolute and relative increase in ear thickness over 7 days of treatment (Figures 4A and 4B). Histological cross-sections of ear skin before and after IMQ treatment revealed enhanced epidermal hyperplasia, a greater disorganization of the stratum corneum, and increased dermal leukocyte infiltration in *CD109*$^{-/-}$ mice relative to the controls (Figure 4C). Consistent with these results, we detected an increased number of both epidermal and dermal γδ17 cells in treated *CD109*$^{-/-}$ mice, even greater than untreated mice (Figures 4D and 4E; cf. Figures 3A and 3B). Notably, the enhanced inflammation persisted in *CD109*$^{-/-}$ mice even after the cessation of IMQ treatment, compared to the control mice (Figure S4). Thus, a loss of CD109 not only disrupts skin homeostasis, but also enhances activation of the IL-23/IL-17 immune axis following overt inflammatory challenge.

CD109 Regulates γδ17 Cells in a Skin-Specific and Cell-Extrinsic Manner

The activation requirements and function of the IL-23/IL-17 immune axis at barrier sites are tissue specific (Lee et al., 2015; Naik et al., 2012) and have important implications for biologics targeting this cellular pathway. To determine whether the absence of CD109 affects the spontaneous activation of γδ17

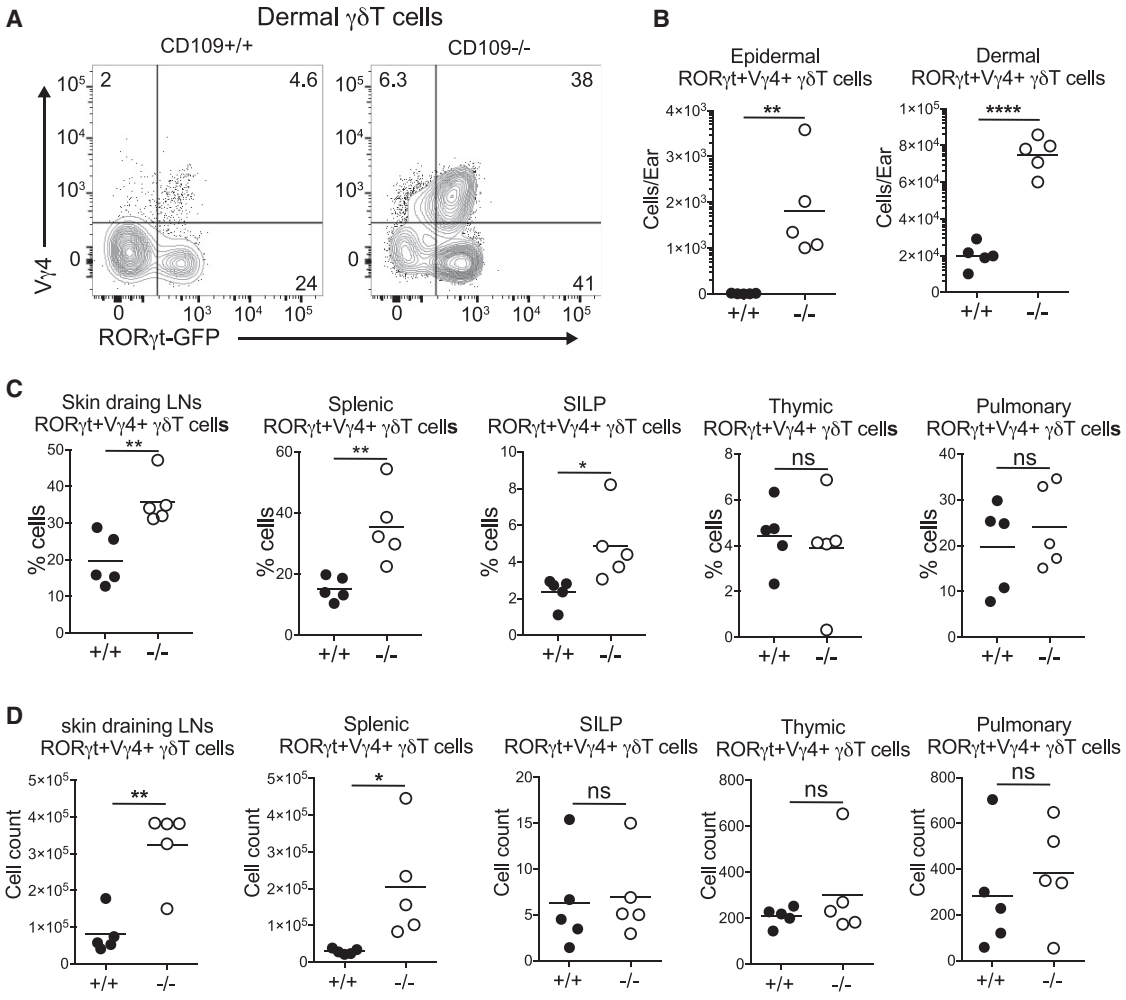

Figure 5. The Activation of γδ17 Cells in the Absence of CD109 Is Tissue Specific

(A) Contour plots showing RORγt-GFP and Vγ4 expression by dermal γδT cells from *RORγt*$^{GFP/+}$*CD109*$^{+/+}$ and *RORγt*$^{GFP/+}$*CD109*$^{-/-}$ ears. Data shown are gated from the dermal CD3^{+}TCRβ^{-}TCRδ^{lo} population. Numbers indicate the frequency of cells within each quadrant.

(B) Total cell counts of epidermal and dermal RORγt^{+}Vγ4^{+} γδT cells.

(C and D) Percentage (C) and total cell counts (D) of RORγt^{+}Vγ4^{+} cells in γδT cells of the skin-draining lymph nodes, spleen, small intestine lamina propria, thymus, and lung tissue. Each circle represents an individual mouse.

(A–D) Data are representative of two independent experiments with 4 or 5 mice/group. (B–D) Unpaired Student's t test; *p < 0.5, **p < 0.01, ****p < 0.0001. ns, not significant.

cells at sites other than the skin, we crossed *CD109*$^{-/-}$ mice to *Rorγt*$^{GFP/+}$ mice that faithfully report all leukocytes with IL-17-producing potential, as indicated above (Ivanov et al., 2009). Consistent with the increased frequency and number of skin γδ17 cells described in Figure 3, the number of Vγ4^{+}GFP^{+} γδ T cells in the epidermis and dermis of *CD109*$^{-/-}$*Rorγt*$^{GFP/+}$ mice was significantly greater than those in control mice (Figures 5A and 5B). We also detected a greater frequency and number of Vγ4^{+}GFP^{+} γδ T cells in the skin-draining lymph nodes (sdLNs) and spleens of *CD109*$^{-/-}$ mice compared to the WT controls (Figures 5C and 5D). In contrast, the number of *GFP*$^{+}$ γδ T cells in other tissues—such as lung, small intestine, mesenteric LN, and thymus—were similar between both groups (Figures 5C and 5D). Similar results were obtained by assessing the number of γδ17 cells upon *in vitro* stimulation of cells from the same tissues (Figure S5). These results are consistent with the robust expression of *Cd109* mRNA expression in keratinocytes, but not epithelial cells from other barrier sites such as the intestine (Figure S6). Taken together, we conclude that CD109 acts in a tissue-specific manner to regulate γδ17 cell homeostasis. Furthermore, these data suggest that CD109 may act in a cell-extrinsic manner to regulate cutaneous γδ17 cells.

To test the cell-extrinsic effects of CD109 on γδ17 cell activation, we first performed *in vitro* cultures in which total skin cells from WT or *CD109*$^{-/-}$ mice were cultured with purified CD3+ T cells from sdLNs (Figure 6A). Stimulation of T cells with IL-1β and IL-23 was used as a positive control to induce IL-17 secretion. T cells cultured with skin from *CD109*$^{-/-}$ mice produced significantly more IL-17A, compared to cultures using WT skin. In line with our *in vivo* studies using anti-IL-23p40 antibody

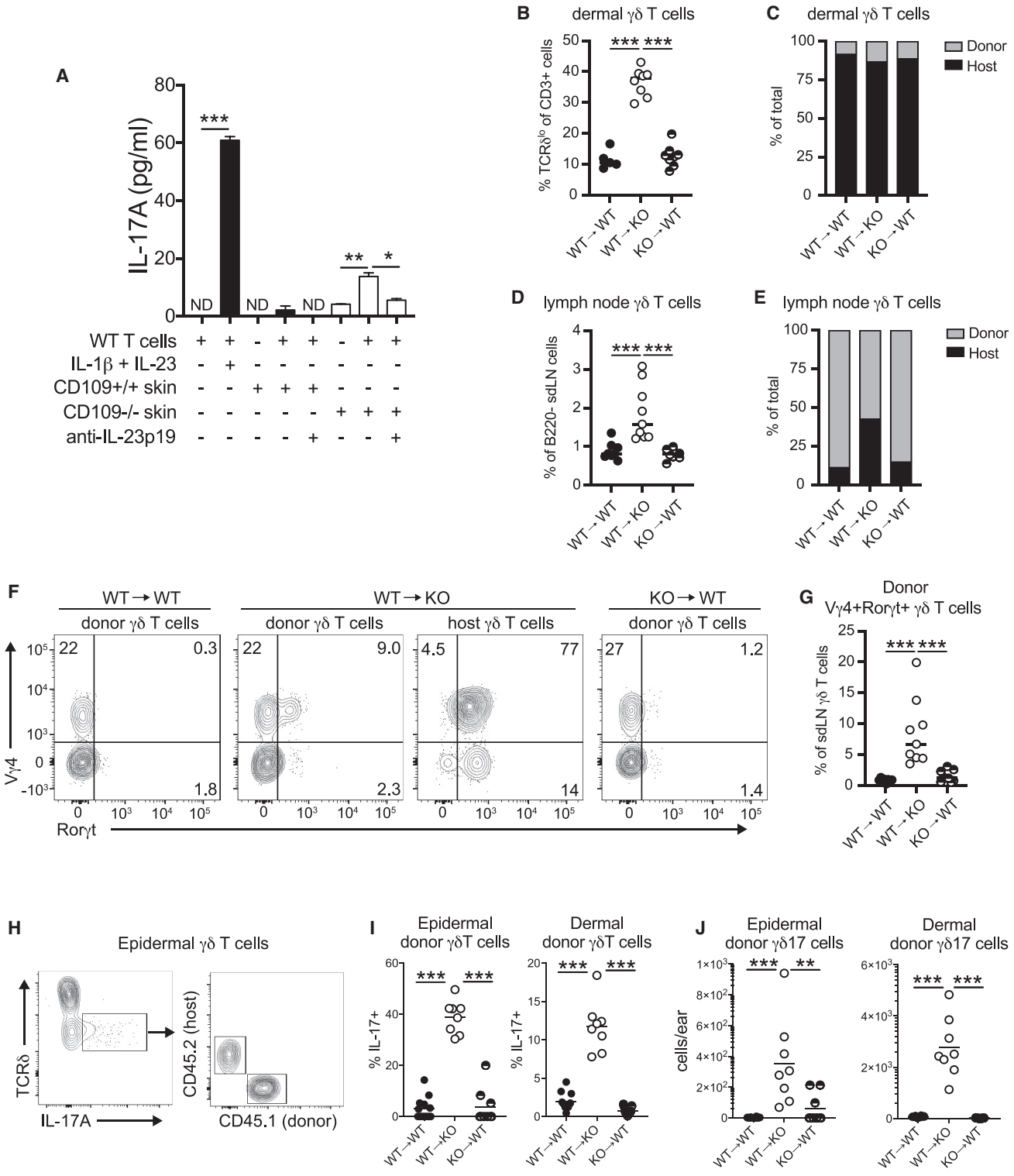

Figure 6. The Activation of γδ17 Cells in the Absence of CD109 Is Cell Extrinsic

(A) Purified T cells from the skin-draining LNs were cultured with skin cells from WT or *CD109*$^{-/-}$ mice in the presence or absence of anti-IL-23p19 antibodies or isotype control. Stimulation of T cells with rIL-1β and rIL-23 was used as a positive control. Supernatants were collected 24 h later, and IL-17A secretion was detected by ELISA.

(legend continued on next page)

treatment (Figure 3J), IL-17A production was abrogated in the presence of anti-IL-23p19 antibodies (Figure 6A). Although dermal γδ T cells have been shown to predominantly accumulate in the dermis within a narrow time period (postnatal days 0–4) and are largely radioresistant (Cai et al., 2014; Sumaria et al., 2011), previous studies have shown that IL-23-dependent inflammation can stimulate the *de novo* generation of γδ17 cells from adult bone marrow (BM) (Muschaweckh et al., 2017; Papotto et al., 2017). To test whether this phenomenon also occurred in *CD109*$^{-/-}$ mice and to confirm the cell-extrinsic regulation of γδ17 cells *in vivo*, we generated BM chimeras in which BM from CD45.1^{+} WT or CD45.2^{+}CD109$^{-/-}$ mice was transplanted into irradiated CD45.2^{+} WT, CD45.1^{+} WT, or *CD109*$^{-/-}$ recipient mice (Figures 6B–6G). Although we observed a selective increase in dermal γδ T cells from the skin of WT → *CD109*$^{-/-}$ chimeras, dermal γδ T cells in all groups were almost exclusively derived from recipient mice, precluding our ability to assess a donor population (Figure 6B and 6C). Although we observed a similar increase in the sdLN of WT → *CD109*$^{-/-}$ chimeras, the majority of γδ T cells from sdLN in all groups were donor derived (Figure 6D). Interestingly, however, WT → *CD109*$^{-/-}$ chimeras contained a substantial number of host-derived γδ T cells that were almost exclusively Vγ4^{+}Rorγt^{+} cells (Figures 6E and 6F). In addition, only WT → *CD109*$^{-/-}$ chimeras harbored *CD45.1*$^{+}$ donor Vγ4^{+} cells expressing Rorγt (Figures 6F and 6G). While these results demonstrated a cell-extrinsic effect on γδ17 cell development, we sought to confirm this observation in skin-resident γδ T cells. To this end, we adopted an approach developed by Gray et al. (2011) in which supplementation of standard BM chimeras with neonatal thymocytes reconstitutes a detectable donor population of dermal γδ T cells. To this end, we co-transplanted adult BM and neonatal thymocytes from *CD45.1*$^{+}$ WT or CD45.2^{+}CD109$^{-/-}$ mice into irradiated CD45.2^{+} WT or *CD109*$^{-/-}$ recipient mice. This approach efficiently reconstituted the skin with a detectable population of donor γδ T cells, as determined by congenic CD45 discrimination (Figure 6H). Consistently, only *CD109*$^{-/-}$ recipients, regardless of donor genotype, exhibited an increase in the frequency and number of epidermal and dermal γδ17 cells (Figures 6I and 6J). Collectively, these results indicate that CD109 expression by a radioresistant cell type acts in a cell-extrinsic manner to limit the activation of cutaneous γδ T cells as well as the *de novo* generation of peripheral γδ17 cells.

CD109 Is Required to Limit γδ17 Cell Activation by Commensal Microbiota

The cell-extrinsic nature of CD109 on γδ17 cell activation prompted us to explore other factors that regulate the cutaneous immune system. The commensal microbial community of the skin, referred to as the microbiota, plays an important role in host defense by promoting anti-microbial peptide secretion by keratinocytes and endowing lymphocytes, including γδ T cells, with the potential to produce IL-17 and protect the host from subsequent infectious challenge (Naik et al., 2012). Consistently, there was a significant increase in anti-microbial gene expression in epidermal and dermal sheets from *CD109*$^{-/-}$ mice, including *S100a7*, *S100a8*, *S100a9*, and *Defb14* mRNA as determined by Nanostring and qRT-PCR analysis, compared to control mice (Figures 7A, 7B, S7A, and S7B). In addition, pathway analysis of our Nanostring data indicated that "cell-cell adhesion" and "defense response to bacterium" were among the top gene sets significantly different between WT and *CD109*$^{-/-}$ epidermal and dermal tissue (Figures 7C and S7C).

To test whether the activation of these pathways was a consequence of alterations to commensal skin microbiota, we performed 16S rRNA sequencing of skin swabs from WT and *CD109*$^{-/-}$ littermates. However, no significant differences at 6 or 12 weeks of age in terms of overall composition, alpha diversity (as determined by Shannon and Faith indices), or beta diversity (e.g., unweighted Unifrac analysis) were observed between genotypes (Figures 7D–7F). An alternate explanation is that CD109 regulates skin permeability, resulting in aberrant exposure or activation to commensal microorganisms. To test skin barrier integrity, we used two approaches. First, an *ex vivo* caffeine diffusion assay was performed in which penetration of caffeine, an amphiphilic small molecule, through the depilated skin is measured in the supernatant by high-performance liquid chromatography (Figure 7G) (Duque-Fernandez et al., 2016). This assay revealed a significant increase in caffeine absorption over time in skin from *CD109*$^{-/-}$ mice compared to WT controls. As an additional measure of barrier integrity, Lucifer yellow, a hydrophilic dye that does not breach the stratum corneum under normal conditions, was applied to depilated mouse back skin sections, and transdermal penetration was quantified by fluorescence spectrophotometry. Similarly, this assay showed that skin from *CD109*$^{-/-}$ mice was significantly more permeable to Lucifer yellow compared to WT control skin (Figure 7H) (Reynier et al., 2016). This difference was age dependent, as no differences in skin barrier permeability were observed using skin from WT and *CD109*$^{-/-}$ neonates (Figure 7I).

Consistent with the aberrant anti-bacterial response and compromised barrier integrity of skin from *CD109*$^{-/-}$ mice, *in situ* mRNA labeling indicated that CD109 transcripts were highly expressed within the basal layer of the epidermis, with a particular abundance in the hair follicles, a site with a dense microbial constituency (Figure 7G) (Kearney et al., 1984; Naik

(B–E) Bone marrow chimeras using either WT or *CD109*$^{-/-}$ donor and recipients were assessed by flow cytometry for (B) the frequency of total dermal γδ T cells, (C) the proportion of host versus donor dermal γδ T cells as determined by congenic CD45 expression, (D) the frequency of total sdLN γδ T cells, and (E) the proportion of host versus donor sdLN γδ T cells as determined by congenic CD45 expression.
(F) Representative contour plots of Vγ4 and Rorγt expression by donor or host TCRβ^{-}TCRδ^{+} γδ T cells from sdLNs of chimeric mice.
(G) The frequency of Vγ4^{+}Rorγt^{+} sdLN γδ T cells from each group of chimeric mice.
(H) Representative contour plots showing total γδ17 cells in reconstituted epidermis (left) containing donor (CD45.1^{+}) and recipient (CD45.2^{+}) cells (right).
(I and J) Frequency and total cell counts of epidermal and dermal donor γδ17 cells from the indicated groups. Each circle represents an individual mouse.
In (A), data are representative of two independent experiments using cells pooled from 5 mice in each experiment. In (B)–(G), data are pooled from two independent experiments with 3–5 mice/group. In (H)–(J), data shown are pooled from two independent experiments with 4 or 5 mice/group. (B–D) Unpaired Student's t test and (F) two-way ANOVA with multiple comparisons; *p < 0.5, **p < 0.01, ***p < 0.001.

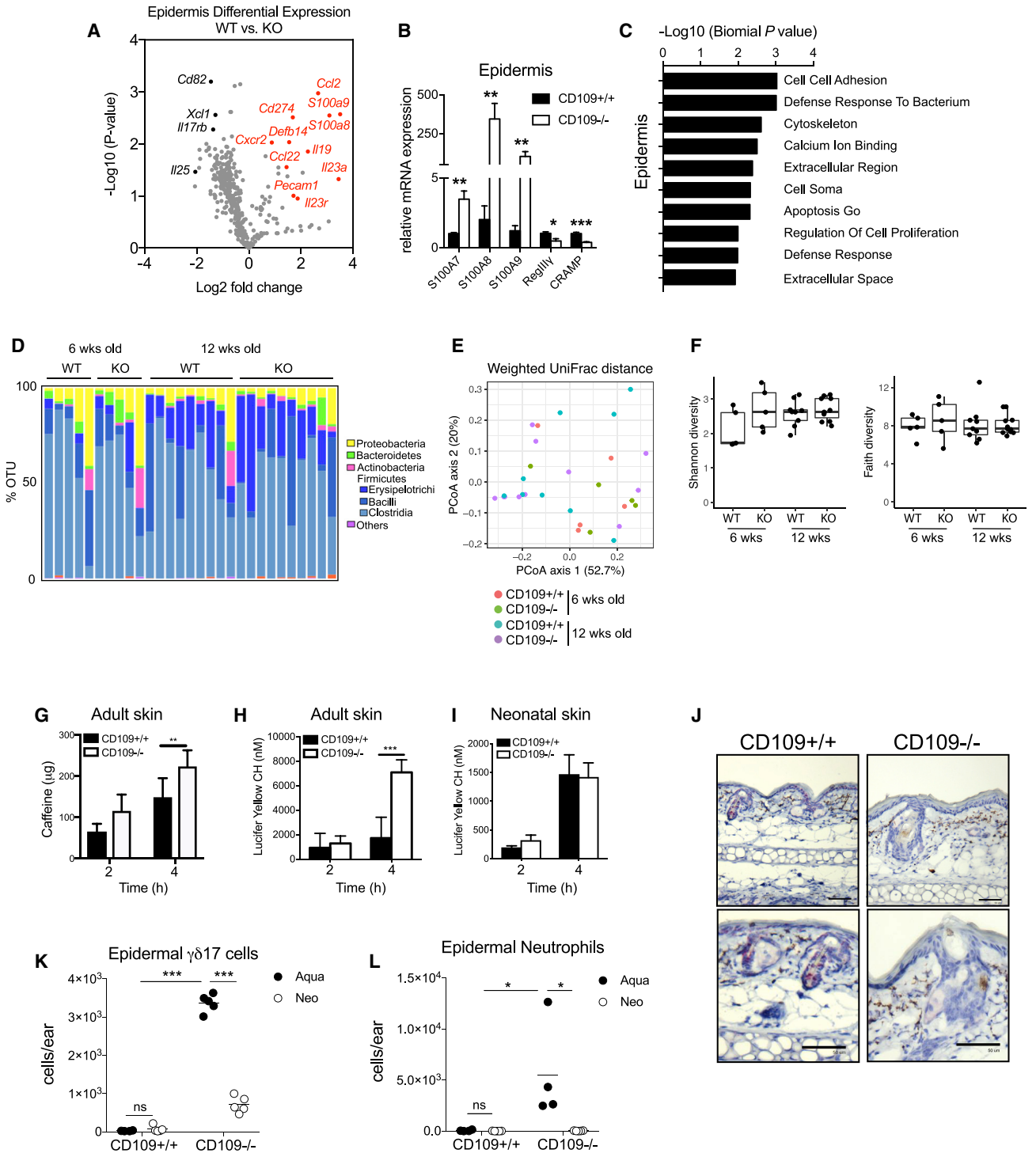

Figure 7. CD109 Regulates Skin Barrier Integrity and γδ17 Cell Activation by the Commensal Microbiota

(A) Volcano plot of gene expression showing the significantly changed genes in epidermis comparing *CD109*$^{-/-}$ versus *CD109*$^{+/+}$ mice. Selected gene names in red denote transcripts associated with anti-microbial function and the IL-23/IL-17 immune axis.

(B) qRT-PCR expression of antimicrobial genes in *CD109*$^{+/+}$ and *CD109*$^{-/-}$ epidermis.

(C) Top 10 significantly increased pathways comparing *CD109*$^{-/-}$ versus *CD109*$^{+/+}$ mice based on advanced nCounter software analysis of epidermal tissue gene expression.

(D–F) 16S rRNA sequencing results from skin swabs of WT and *CD109*$^{-/-}$ littermates at 6 and 12 weeks of age. Bars and dots represent individual mice.

(legend continued on next page)

et al., 2012). To directly test whether the commensal microbiota is required for the activation of the IL-23/IL-17 axis in *CD109*$^{-/-}$ mice, we topically applied broad-spectrum antibiotics or a vehicle control to the ear skin of WT and *CD109*$^{-/-}$ skin, and cutaneous γδ17 cell numbers and neutrophil accumulation were used as readouts. Remarkably, short-term treatment of *CD109*$^{-/-}$ mice with antibiotics abrogated the epidermal accumulation of γδ17 cells, restored the number of dermal γδ17 cells to WT numbers, and eliminated epidermal neutrophil accumulation (Figures 7H, 7I, and S7D). Consistently, *Il17a* and *S100a8* mRNA in *CD109*$^{-/-}$ skin was also significantly reduced after antibiotic treatment, while *Il23a* expression and pSTAT3 activation remained elevated (Figures S7E–S7H).

DISCUSSION

Immune cells residing in barrier tissues such as the skin, lung, intestine, and female reproductive tract face the complex task of protecting the host from pathogens while living in a mutualistic relationship with the commensal microbiota. However, the primary function of the immune system is to recognize and destroy microorganisms. Therefore, mechanisms that counter or temper this function at barrier sites must be put in place to tolerate the microbial shield that maximizes host fitness in a dynamic environment. While several cell-intrinsic pathways have been described that limit cutaneous immune cell proliferation and activation, the molecular mechanisms by which structural cells negatively regulate the immune system are less understood. Here, we identify CD109 as a negative regulator of the IL-23/IL-17 immune axis and γδ17 cell reactivity to the cutaneous microbiota. Consistent with the critical role of this immune axis in psoriasiform inflammation (Gaffen et al., 2014), deletion of CD109 led to enhanced disease severity following IMQ-induced sensitization. Although CD109 has been shown to be expressed by activated human T cells (Sutherland et al., 1991), our results indicate a cell-extrinsic role for regulating the localization and production of IL-17 by γδ T cells (Muschaweckh et al., 2017; Papotto et al., 2017). By contrast, no dysregulation of γδ17 cells was apparent at the other barrier sites examined, including the gut and lung. While it will be important to investigate the role of CD109 during overt inflammation at these alternative barrier sites, our data point toward a tissue-specific function for CD109 in regulating skin homeostasis.

Prior to our study, little was known regarding the role of CD109 in cutaneous immune regulation. Although Mii et al. (2012) found an accumulation of leukocytes in the skin of *CD109*$^{-/-}$ mice, the immune pathways activated *in vivo* and the mechanisms driving inflammation were not examined. Our studies show that the deletion of CD109 in mice results in dysregulated keratinocyte activation and spontaneous activation of the cutaneous IL-23/IL-17 immune axis, including neutrophil accumulation, increased expression of alarmins with anti-microbial properties such as S100A7, S100A8, and S100A9 and multiple cytokines previously associated with psoriatic skin inflammation, including members of the IL-20R-dependent cytokine family such as IL-19 and IL-20, that signal via STAT3-dependent pathways. Consistently, we found constitutive activation of STAT3 in *CD109*$^{-/-}$ skin lysates even in the absence of *ex vivo* stimulation. Interestingly, STAT3 activation was not associated with increased age, as were other readouts of inflammation, including hair loss and alarmin expression. Although dysregulated STAT3 activation in keratinocytes is strongly associated with the IL-23/IL-17 immune axis and psoriasiform inflammation (Sano et al., 2005), STAT3-dependent signals are downstream of numerous cytokines, some of which can exert anti-inflammatory effects, most notably IL-10. A comprehensive analysis of how STAT3-dependent cytokine expression may change with age would need to be performed to understand the signals driving this pathway in the absence of CD109.

While we cannot equate our animal studies with human disease, a previous study showed decreased protein production of CD109 within psoriasis lesions compared to non-lesional skin from the same patients (Litvinov et al., 2011). However, genomic analyses of patients with psoriasis have yet to identify risk alleles in the CD109 gene. This may not be surprising, however, as no change was observed in *cd109* mRNA expression between skin from patients with psoriasis and healthy controls (Litvinov et al., 2011). Although these clinical results are based on small patient cohorts, they suggest that post-translation modification of CD109 may be a critical determinant of disease initiation and/or progression and may provide the impetus for understanding how CD109 is regulated.

Deletion of CD109 was prominently associated with the accumulation of γδ17 cells, a population previously implicated in early protective immunity to extracellular bacterial and fungal infection, but also potential initiators of pathological skin inflammatory conditions as in the case of psoriasis (Cai et al., 2011; Cho et al., 2010; Kashem et al., 2015; Laggner et al., 2011). Sandrock et al. (2018) recently described the aberrant localization of dermal-derived γδ17 cells to the epidermis in the context of IMQ-induced inflammation, a result we also observed (Sandrock et al., 2018). However, in accordance with the inflammatory nature of *CD109*$^{-/-}$ skin, we observed the spontaneous accumulation of γδ17 cells in the epidermal layer even in the absence of intentional immune challenge. In our analysis of Vγ4^{+} γδ T cell

(D) Bacterial phyla composition based on operational taxonomic unit (OTU) annotation.
(E) Principal component analysis using weighted UniFrac analysis.
(F) Box plots showing beta diversity of all groups using Shannon and Faith indices.
(G–I) *In vitro* percutaneous absorption of caffeine (G) and Lucifer yellow (H and I) by adult (G and H) and neonatal (I) skin at 2 and 4 h post-exposure.
(J) RNAScope of CD109 transcripts in *CD109*$^{+/+}$ and *CD109*$^{-/-}$ ear skin. Red dots indicate *Cd109* mRNA. Scale bar: 50 μm.
(K and L) Total cell counts of epidermal γδ17 cells and neutrophils following 7 days of Aquaphor or Neosporin treatment.
Data shown represent one (I), two (B, G, and H), or three (K and L) independent experiments with at least 3 mice per group. Nanostring data (A and C) is from one experiment containing 3 mice/group. Each circle in the scatterplots represents an individual mouse. Aqua, Aquaphor; Neo, Neosporin; ND, undetected. Unpaired Student's t test; **p < 0. 01, ***p < 0.001. Two-way ANOVA with multiple comparisons; *p < 0.05 and **p < 0. 01.

localization, a subset enriched for IL-17 production, we observed the preferential localization of these cells around the hair follicle. Recent data indicate that this region of the epidermis is particularly immunologically active, as these sites are also enriched for $CD4^+$ T regulatory cells (Tregs) that promote the hair cycle and serve as a conduit for the capture of epicutaneous antigens by dermal dendritic cells (Scharschmidt et al., 2017; Tordesillas et al., 2018). In addition, hair follicles are migration portals for monocytes to reconstitute the epidermal Langerhans cell population during tissue stress (Nagao et al., 2012). Notably, Treg and Langerhans cell expression of CCR6 is required for accumulation at the follicle (Nagao et al., 2012; Scharschmidt et al., 2017). Similarly, CCR6 is highly expressed on dermal γδ17 cells and is required for IMQ-induced psoriasiform inflammation (Gray et al., 2013). Consistent with these data, we observed prominent expression of CD109 within the hair follicle and, following its deletion, progressive hair loss and a concomitant increase of CCL20 expression, the ligand for CCR6, in epidermal sheets. Thus, CD109 may act as a rheostat to balance CCL20-CCR6-dependent regulatory and inflammatory immune elements to mediate barrier homeostasis and tissue regeneration at the hair follicle.

CD109 has been reported as a TGF-β co-receptor and negative regulator of canonical TGF-β signaling (Litvinov et al., 2011). Consistent with the phenotype of *CD109*$^{-/-}$ mice, overexpression of TGF-β signaling in basal keratinocytes results in aberrant epidermal thickening and IL-17 production (Li et al., 2004). However, examining SMAD2/3 activation of total skin cells, we were unable to detect differences in responsiveness to TGF-β signaling as determined by phosphorylated SMAD2/3. Although these results do not rule out a potential role for CD109 in regulating TGF-β signaling in certain conditions, our data suggest that CD109 may have additional and/or alternative roles in cutaneous immune regulation. We found CD109 to be highly expressed in the basal layer of the epidermis and the hair follicle. We chose to examine the location of CD109 mRNA expression by *in situ* mRNA detection because, once translated, its GPI anchor is sensitive to phospholipase cleavage, resulting in a soluble protein, making its cellular source difficult to determine (Litvinov et al., 2011). Although our histological and imaging results indicated epidermal hyperplasia and aberrant skin thickening in the absence of CD109, whether this protein directly regulates keratinocyte proliferation and the specific stage of cell differentiation that CD109 becomes functionally active remain to be determined. Interestingly, CD109 has been demonstrated to localize to lamellar bodies, lipid-rich vesicles secreted by granular keratinocytes that join corneocytes at the most superficial region of the stratum corneum and are critical for barrier formation (Raymond et al., 2008). We are currently investigating whether CD109 activity promotes the formation and/or function of lamellar bodies to fortify the skin barrier (Elias, 2007).

Despite the low microbial biomass compared to other barrier tissues such as the intestine, it is well established that microbes residing on mammalian skin condition the cutaneous immune system to respond toward a host of environmental challenges (Byrd et al., 2018). Indeed, microbial colonization of the skin regulates the susceptibility to diverse pathogens as well as infection-induced tissue damage (Boldock et al., 2018; Naik et al., 2012). Thus, limiting reactivity to microbiota-dependent inflammation is central to orchestrating a balanced immune response. Our results indicate that CD109 limits the expression of anti-microbial factors, including members of the S100 and β-defensin families. Importantly, a brief course of topical antibiotics to *CD109*$^{-/-}$ mice was sufficient to reduce the number of γδ17 cells and neutrophils to numbers comparable to WT mice. These results indicate that continuous exposure to the microbiota is required to drive activation of IL-17-producing cells in this context. Although our *in vitro* and *in vivo* experiments indicate that IL-23 is an important driver of dysregulated IL-17 production in CD109-deficient mice, IL-23 expression remained elevated in antibiotic-treated *CD109*$^{-/-}$ mice. One explanation for these disparate results is that our methods of *il23a* mRNA detection are not sufficiently sensitive to observe small changes in transcription. An alternate and more interesting possibility is that the imprinting of IL-23-expressing cells such as dendritic cells, macrophages, or even keratinocytes (Cai et al., 2011; Yoon et al., 2016) may not be affected during the brief course of antibiotics we administered. Consistent with this idea are recent findings demonstrating skin epithelial stem cells that give rise to mature keratinocytes retain a "memory" of tissue injury after the resolution of inflammation, resulting in persistent gene expression modules related to cytokine production (Naik et al., 2017). Although the mechanisms by which microbial colonization of the epidermis transmits signals to the dermal immune compartment are not well understood, the signals stimulating IL-17 production in this context are likely cytokine driven and not antigen restricted because (1) both $Vγ4^+$ and $Vγ4^-$ γδ T cell subsets produced increased amounts of IL-17 in the absence of CD109; (2) production of IL-17 by γδ T cells does not require TCR engagement; and (3) we did not detect any spontaneous cytokine production by cutaneous αβ T cells, a lineage that requires antigen encounter for activation. As we found no significant differences in the microbiomes of skin from WT and *CD109*$^{-/-}$ mice, our data suggest that CD109 regulates the response to the skin microbiota rather than altering the microbiota itself. A more likely explanation for the aberrant response is that a compromised barrier integrity in *CD109*$^{-/-}$ mice leads to increased infiltration and/or access of microbial antigens to the deeper layers of the skin, resulting in enhanced activation of the existing dermal immune compartment. Indeed, microbial DNA has been observed in the dermal and skin adipose tissues even under steady-state conditions (Nakatsuji et al., 2013).

Based on our data, we propose a scenario whereby the absence of CD109 production by keratinocytes results in an age-associated breach of the skin barrier sufficient to expose the dermal immune compartment to chronic stimulation by epicutaneous commensal microbes. Dermal-infiltrating microbes or microbial-derived products are subsequently sensed by pattern recognition receptor-expressing innate effector cells—such as dermal dendritic cells, macrophages, or possibly keratinocytes themselves (Naik et al., 2015; Yoon et al., 2016)—that release inflammatory cytokines promoting neutrophil recruitment and IL-23-dependent proliferation and activation of dermal-derived γδ17 cells that act on the keratinocytes to induce epidermal hyperplasia. A compromised barrier also stimulates an epidermal stress response inducing CCL20 that promotes

γδ17 cell migration to the hair follicle, a position that predisposes the host to enhanced reactivity toward overt inflammatory stimuli such as IMQ. Identifying CD109 as an endogenous regulator of cutaneous inflammation and host tolerance to the microbiota motivates further investigations into tissue-specific mechanisms that maintain tissue homeostasis and skin health.

STAR★METHODS

Detailed methods are provided in the online version of this paper and include the following:

- KEY RESOURCES TABLE
- LEAD CONTACT AND MATERIALS AVAILABILITY
- EXPERIMENTAL MODEL AND SUBJECT DETAILS
- METHOD DETAILS
  - Immunoblots
  - Histology and RNA scope
  - Isolation of skin cells
  - Flow cytometry
  - Skin-T cell co-cultures
  - Tissue processing and confocal microscopy
  - Quantitative RT-PCR analyses
  - Nanostring analysis
  - Anti-IL-12/23p40 administration
  - Imiquimod-induced skin inflammation
  - Topical antibiotic treatment and 16S rRNA quantification
  - ELISA
  - Bone marrow chimera generation
  - Percutaneous absorption studies
  - 16S rRNA sequencing of skin microbiota
- QUANTIFICATION AND STATISTICAL ANALYSIS
- DATA AND CODE AVAILABILITY

SUPPLEMENTAL INFORMATION

Supplemental Information can be found online at https://doi.org/10.1016/j.celrep.2019.09.003.

ACKNOWLEDGMENTS

We thank members of the King Laboratory and collaborators for their critical reading of the manuscript and the McGill Integrated Core for Animal Modeling for embryo cryorecovery of *CD109*$^{-/-}$ mice. We are also grateful to the Children's Hospital of Philadelphia Microbiome Center, especially Dr. Jung-Jin Lee, for their assistance with skin microbiome sequencing and analysis. H.Z. is a recipient of a Chinese Scholarship Council Award. N.K. is a recipient of a Fonds de recherche du Québec - Santé (FRQS) Postdoctoral Fellowship. I.L.K. is a Canada Research Chair in Barrier Immunity. This work was supported by a Discovery Grant from the Natural Sciences and Engineering Research Council of Canada (RGPIN-2015-05491) and a Canadian Institutes of Health Research Project Grant (PJT-148552) awarded to I.L.K.

AUTHOR CONTRIBUTIONS

H.Z. and G.C. designed and performed experiments, analyzed the data, and wrote the manuscript. B.P. performed the RNAscope experiments. N.K. performed tissue harvests and analyzed data. M.E.G. performed cell-sorting experiments and qPCR analysis of intestinal tissue. G.F. assisted with experiments, performed western blots, and provided critical technical input. D.C.V. provided reagents and intellectual input. B.T. performed the qRT-PCR for inflammatory gene expression and skin microbiome analysis. M.S. performed percutaneous absorption assays. R.P. provided technical support and intellectual input for the percutaneous studies. I.L.K. conceptualized the study, designed and performed experiments, and wrote the manuscript.

DECLARATION OF INTERESTS

The authors declare no competing interests.

Received: March 28, 2019
Revised: July 26, 2019
Accepted: August 30, 2019
Published: October 8, 2019

REFERENCES

Becher, B., and Pantelyushin, S. (2012). Hiding under the skin: Interleukin-17-producing γδ T cells go under the skin? Nat. Med. *18*, 1748–1750.

Boldock, E., Surewaard, B.G.J., Shamarina, D., Na, M., Fei, Y., Ali, A., Williams, A., Pollitt, E.J.G., Szkuta, P., Morris, P., et al. (2018). Human skin commensals augment Staphylococcus aureus pathogenesis. Nat. Microbiol. *3*, 881–890.

Byrd, A.L., Belkaid, Y., and Segre, J.A. (2018). The human skin microbiome. Nat. Rev. Microbiol. *16*, 143–155.

Cai, Y., Shen, X., Ding, C., Qi, C., Li, K., Li, X., Jala, V.R., Zhang, H.G., Wang, T., Zheng, J., and Yan, J. (2011). Pivotal role of dermal IL-17-producing γδ T cells in skin inflammation. Immunity *35*, 596–610.

Cai, Y., Xue, F., Fleming, C., Yang, J., Ding, C., Ma, Y., Liu, M., Zhang, H.G., Zheng, J., Xiong, N., and Yan, J. (2014). Differential developmental requirement and peripheral regulation for dermal Vγ4 and Vγ6T17 cells in health and inflammation. Nat. Commun. *5*, 3986.

Callahan, B.J., McMurdie, P.J., Rosen, M.J., Han, A.W., Johnson, A.J., and Holmes, S.P. (2016). DADA2: High-resolution sample inference from Illumina amplicon data. Nat. Methods *13*, 581–583.

Cho, J.S., Pietras, E.M., Garcia, N.C., Ramos, R.I., Farzam, D.M., Monroe, H.R., Magorien, J.E., Blauvelt, A., Kolls, J.K., Cheung, A.L., et al. (2010). IL-17 is essential for host defense against cutaneous Staphylococcus aureus infection in mice. J. Clin. Invest. *120*, 1762–1773.

Chuang, C.H., Greenside, P.G., Rogers, Z.N., Brady, J.J., Yang, D., Ma, R.K., Caswell, D.R., Chiou, S.H., Winters, A.F., Grüner, B.M., et al. (2017). Molecular definition of a metastatic lung cancer state reveals a targetable CD109-Janus kinase-Stat axis. Nat. Med. *23*, 291–300.

Duque-Fernandez, A., Gauthier, L., Simard, M., Jean, J., Gendreau, I., Morin, A., Soucy, J., Auger, M., and Pouliot, R. (2016). A 3D-psoriatic skin model for dermatological testing: The impact of culture conditions. Biochem. Biophys. Rep. *8*, 268–276.

Elias, P.M. (2007). The skin barrier as an innate immune element. Semin. Immunopathol. *29*, 3–14.

Fuchs, E., and Nowak, J.A. (2008). Building epithelial tissues from skin stem cells. Cold Spring Harb. Symp. Quant. Biol. *73*, 333–350.

Gaffen, S.L., Jain, R., Garg, A.V., and Cua, D.J. (2014). The IL-23-IL-17 immune axis: from mechanisms to therapeutic testing. Nat. Rev. Immunol. *14*, 585–600.

Gray, E.E., Suzuki, K., and Cyster, J.G. (2011). Cutting edge: Identification of a motile IL-17-producing gammadelta T cell population in the dermis. J. Immunol. *186*, 6091–6095.

Gray, E.E., Ramírez-Valle, F., Xu, Y., Wu, S., Wu, Z., Karjalainen, K.E., and Cyster, J.G. (2013). Deficiency in IL-17-committed Vγ4(+) γδ T cells in a spontaneous Sox13-mutant CD45.1(+) congenic mouse substrain provides protection from dermatitis. Nat. Immunol. *14*, 584–592.

Heilig, J.S., and Tonegawa, S. (1986). Diversity of murine gamma genes and expression in fetal and adult T lymphocytes. Nature *322*, 836–840.

Ivanov, I.I., Atarashi, K., Manel, N., Brodie, E.L., Shima, T., Karaoz, U., Wei, D., Goldfarb, K.C., Santee, C.A., Lynch, S.V., et al. (2009). Induction of intestinal Th17 cells by segmented filamentous bacteria. Cell *139*, 485–498.

Kashem, S.W., Riedl, M.S., Yao, C., Honda, C.N., Vulchanova, L., and Kaplan, D.H. (2015). Nociceptive Sensory Fibers Drive Interleukin-23 Production from CD301b+ Dermal Dendritic Cells and Drive Protective Cutaneous Immunity. Immunity *43*, 515–526.

Katoh, K., and Standley, D.M. (2013). MAFFT multiple sequence alignment software version 7: improvements in performance and usability. Mol. Biol. Evol. *30*, 772–780.

Kearney, J.N., Harnby, D., Gowland, G., and Holland, K.T. (1984). The follicular distribution and abundance of resident bacteria on human skin. J. Gen. Microbiol. *130*, 797–801.

Kerkhoff, C., Voss, A., Scholzen, T.E., Averill, M.M., Zänker, K.S., and Bornfeldt, K.E. (2012). Novel insights into the role of S100A8/A9 in skin biology. Exp. Dermatol. *21*, 822–826.

Laggner, U., Di Meglio, P., Perera, G.K., Hundhausen, C., Lacy, K.E., Ali, N., Smith, C.H., Hayday, A.C., Nickoloff, B.J., and Nestle, F.O. (2011). Identification of a novel proinflammatory human skin-homing Vγ9Vδ2 T cell subset with a potential role in psoriasis. J. Immunol. *187*, 2783–2793.

Lee, J.S., Tato, C.M., Joyce-Shaikh, B., Gulen, M.F., Cayatte, C., Chen, Y., Blumenschein, W.M., Judo, M., Ayanoglu, G., McClanahan, T.K., et al. (2015). Interleukin-23-Independent IL-17 Production Regulates Intestinal Epithelial Permeability. Immunity *43*, 727–738.

Li, A.G., Wang, D., Feng, X.H., and Wang, X.J. (2004). Latent TGFbeta1 overexpression in keratinocytes results in a severe psoriasis-like skin disorder. EMBO J. *23*, 1770–1781.

Litvinov, I.V., Bizet, A.A., Binamer, Y., Jones, D.A., Sasseville, D., and Philip, A. (2011). CD109 release from the cell surface in human keratinocytes regulates TGF-β receptor expression, TGF-β signalling and STAT3 activation: relevance to psoriasis. Exp. Dermatol. *20*, 627–632.

Mii, S., Murakumo, Y., Asai, N., Jijiwa, M., Hagiwara, S., Kato, T., Asai, M., Enomoto, A., Ushida, K., Sobue, S., et al. (2012). Epidermal hyperplasia and appendage abnormalities in mice lacking CD109. Am. J. Pathol. *181*, 1180–1189.

Mii, S., Hoshino, A., Enomoto, A., Murakumo, Y., Ito, M., Yamaguchi, A., and Takahashi, M. (2018). CD109 deficiency induces osteopenia with an osteoporosis-like phenotype in vivo. Genes Cells *23*, 590–598.

Muschaweckh, A., Petermann, F., and Korn, T. (2017). IL-1β and IL-23 Promote Extrathymic Commitment of $CD27^{+}CD122^{-}$ γδ T Cells to γδT17 Cells. J. Immunol. *199*, 2668–2679.

Nagao, K., Kobayashi, T., Moro, K., Ohyama, M., Adachi, T., Kitashima, D.Y., Ueha, S., Horiuchi, K., Tanizaki, H., Kabashima, K., et al. (2012). Stress-induced production of chemokines by hair follicles regulates the trafficking of dendritic cells in skin. Nat. Immunol. *13*, 744–752.

Naik, S., Bouladoux, N., Wilhelm, C., Molloy, M.J., Salcedo, R., Kastenmuller, W., Deming, C., Quinones, M., Koo, L., Conlan, S., et al. (2012). Compartmentalized control of skin immunity by resident commensals. Science *337*, 1115–1119.

Naik, S., Bouladoux, N., Linehan, J.L., Han, S.J., Harrison, O.J., Wilhelm, C., Conlan, S., Himmelfarb, S., Byrd, A.L., Deming, C., et al. (2015). Commensal-dendritic-cell interaction specifies a unique protective skin immune signature. Nature *520*, 104–108.

Naik, S., Larsen, S.B., Gomez, N.C., Alaverdyan, K., Sendoel, A., Yuan, S., Polak, L., Kulukian, A., Chai, S., and Fuchs, E. (2017). Inflammatory memory sensitizes skin epithelial stem cells to tissue damage. Nature *550*, 475–480.

Nakatsuji, T., Chiang, H.I., Jiang, S.B., Nagarajan, H., Zengler, K., and Gallo, R.L. (2013). The microbiome extends to subepidermal compartments of normal skin. Nat. Commun. *4*, 1431.

Nielsen, M.M., Witherden, D.A., and Havran, W.L. (2017). γδ T cells in homeostasis and host defence of epithelial barrier tissues. Nat. Rev. Immunol. *17*, 733–745.

Papotto, P.H., Gonçalves-Sousa, N., Schmolka, N., Iseppon, A., Mensurado, S., Stockinger, B., Ribot, J.C., and Silva-Santos, B. (2017). IL-23 drives differentiation of peripheral γδ17 T cells from adult bone marrow-derived precursors. EMBO Rep. *18*, 1957–1967.

Price, M.N., Dehal, P.S., and Arkin, A.P. (2010). FastTree 2–approximately maximum-likelihood trees for large alignments. PLoS ONE *5*, e9490.

Raymond, A.A., Gonzalez de Peredo, A., Stella, A., Ishida-Yamamoto, A., Bouyssie, D., Serre, G., Monsarrat, B., and Simon, M. (2008). Lamellar bodies of human epidermis: proteomics characterization by high throughput mass spectrometry and possible involvement of CLIP-170 in their trafficking/secretion. Mol. Cell. Proteomics *7*, 2151–2175.

Reynier, M., Allart, S., Gaspard, E., Moga, A., Goudounèche, D., Serre, G., Simon, M., and Leprince, C. (2016). Rab11a Is Essential for Lamellar Body Biogenesis in the Human Epidermis. J. Invest. Dermatol. *136*, 1199–1209.

Ribot, J.C., deBarros, A., Pang, D.J., Neves, J.F., Peperzak, V., Roberts, S.J., Girardi, M., Borst, J., Hayday, A.C., Pennington, D.J., and Silva-Santos, B. (2009). CD27 is a thymic determinant of the balance between interferon-gamma- and interleukin 17-producing gammadelta T cell subsets. Nat. Immunol. *10*, 427–436.

Ridaura, V.K., Bouladoux, N., Claesen, J., Chen, Y.E., Byrd, A.L., Constantinides, M.G., Merrill, E.D., Tamoutounour, S., Fischbach, M.A., and Belkaid, Y. (2018). Contextual control of skin immunity and inflammation by *Corynebacterium*. J. Exp. Med. *215*, 785–799.

Sandrock, I., Reinhardt, A., Ravens, S., Binz, C., Wilharm, A., Martins, J., Oberdörfer, L., Tan, L., Lienenklaus, S., Zhang, B., et al. (2018). Genetic models reveal origin, persistence and non-redundant functions of IL-17-producing γδ T cells. J. Exp. Med. *215*, 3006–3018.

Sano, S., Chan, K.S., Carbajal, S., Clifford, J., Peavey, M., Kiguchi, K., Itami, S., Nickoloff, B.J., and DiGiovanni, J. (2005). Stat3 links activated keratinocytes and immunocytes required for development of psoriasis in a novel transgenic mouse model. Nat. Med. *11*, 43–49.

Scharschmidt, T.C., Vasquez, K.S., Pauli, M.L., Leitner, E.G., Chu, K., Truong, H.A., Lowe, M.M., Sanchez Rodriguez, R., Ali, N., Laszik, Z.G., et al. (2017). Commensal Microbes and Hair Follicle Morphogenesis Coordinately Drive Treg Migration into Neonatal Skin. Cell Host Microbe. *21*, 467–477.e465.

Sumaria, N., Roediger, B., Ng, L.G., Qin, J., Pinto, R., Cavanagh, L.L., Shklovskaya, E., Fazekas de St Groth, B., Triccas, J.A., and Weninger, W. (2011). Cutaneous immunosurveillance by self-renewing dermal gammadelta T cells. J. Exp. Med. *208*, 505–518.

Sutherland, D.R., Yeo, E., Ryan, A., Mills, G.B., Bailey, D., and Baker, M.A. (1991). Identification of a cell-surface antigen associated with activated T lymphoblasts and activated platelets. Blood *77*, 84–93.

Sutton, C.E., Lalor, S.J., Sweeney, C.M., Brereton, C.F., Lavelle, E.C., and Mills, K.H. (2009). Interleukin-1 and IL-23 induce innate IL-17 production from gammadelta T cells, amplifying Th17 responses and autoimmunity. Immunity *31*, 331–341.

Tordesillas, L., Lozano-Ojalvo, D., Dunkin, D., Mondoulet, L., Agudo, J., Merad, M., Sampson, H.A., and Berin, M.C. (2018). $PDL2^{+}$ $CD11b^{+}$ dermal dendritic cells capture topical antigen through hair follicles to prime LAP^{+} Tregs. Nat. Commun. *9*, 5238.

van der Fits, L., Mourits, S., Voerman, J.S., Kant, M., Boon, L., Laman, J.D., Cornelissen, F., Mus, A.M., Florencia, E., Prens, E.P., and Lubberts, E. (2009). Imiquimod-induced psoriasis-like skin inflammation in mice is mediated via the IL-23/IL-17 axis. J. Immunol. *182*, 5836–5845.

Yoon, J., Leyva-Castillo, J.M., Wang, G., Galand, C., Oyoshi, M.K., Kumar, L., Hoff, S., He, R., Chervonsky, A., Oppenheim, J.J., et al. (2016). IL-23 induced in keratinocytes by endogenous TLR4 ligands polarizes dendritic cells to drive IL-22 responses to skin immunization. J. Exp. Med. *213*, 2147–2166.

STAR★METHODS

KEY RESOURCES TABLE

REAGENT or RESOURCE	SOURCE	IDENTIFIER
Antibodies		
Mouse monoclonal anti-mouse CD45.1-eFluor 450 (A20)	eBioscience	Cat# 48-0453-82; RRID: AB_1272189
Mouse monoclonal anti-mouse CD45.2-PE-eFluor 610 (104)	eBioscience	Cat# 61-0454-82; RRID: AB_2574562
Rat monoclonal anti-mouse B220-Alexa Fluor 700 (RA3-6B2)	eBioscience	Cat# 56-0452-80; RRID: AB_891460
Hamster monoclonal anti-Mouse CD3e-BV650 (145-2C11)	BD	Cat# 564378; RRID: AB_2738779
Hamster monoclonal anti-Mouse TCRβ-APC-eFluor 780 (H57-597)	eBioscience	Cat# 47-5961-8; RRID: AB_1272173
Hamster monoclonal anti-Mouse TCRγ/δ-FITC (GL3)	Biolegend	Cat# 118106; RRID: AB_313830
Hamster monoclonal anti-Mouse TCRγ/δ-PE (GL3)	Biolegend	Cat# 118108; RRID: AB_313832
Hamster monoclonal anti-Mouse TCRγ/δ-PerCP/Cy5.5 (GL3)	Biolegend	Cat# 118118; RRID: AB_10612756
Hamster monoclonal anti-Mouse TCR Vγ2(4)-PE-Cyanine7 (UC3-10A6)	eBioscience	Cat# 25-5828-82; RRID: AB_2573474
Hamster monoclonal anti-Mouse TCR Vγ2(4)-PE (UC3-10A6)	Biolegend	Cat# 137706; RRID: AB_10643577
Rat monoclonal anti-mouse IL-17a-PE (eBio17B7)	eBioscience	Cat# 12-7177-81; RRID: AB_763582
Rat monoclonal anti-mouse IFN-γ-Alexa Fluor 488 (XMG1.2)	eBioscience	Cat# 53-7311-82; RRID: AB_469932
Rat monoclonal anti-mouse Ki-67-FITC (SolA15)	eBioscience	Cat# 11-5698-82; RRID: AB_11151330
Rat monoclonal anti-mouse Ly6G-Alexa Fluor 488 (1A8-Ly6g)	eBioscience	Cat # 11-9668-82; RRID: AB_2572532
Rat monoclonal anti-mouse CD11-APC (M1/70)	eBioscience	Cat# 17-0112-82; RRID: AB_469343
Mouse CD109 Affinity Purified Polyclonal Ab	R&D	Cat# AF7717
Mouse monoclonal anti-mouse Lamin B1 (A11)	Santa Cruz	Cat# sc-377000
Goat Anti-Rabbit IgG (H + L)-HRP Conjugate	BioRad	Cat# 170-6515
Goat Anti-Mouse IgG (H + L)-HRP Conjugate	BioRad	Cat# 170-6516
Rabbit Anti-Sheep IgG (H+L)-HRP Conjugate	BioRad	Cat# 1721017
Phospho-stat3 (Tyr705) rabbit mAb (D3A7)	Cell signaling	Cat# 9145S
Stat3 mouse mAb (124H6)	Cell signaling	Cat# 9139S
Phospho-smad2 (Ser465/467)/Smad3 (Ser423/425) Rabbit mAb (D27F4)	Cell signaling	Cat# 8828S
Smad2/3 Rabbit mAb (D7G7)	Cell signaling	Cat# 8685S;
Rat *InVivo*mAb anti-mouse IL-12 p40 (C17.8)	BioXell	Cat# BE0051; RRID: AB_1107698
*InVivo*mAb rat IgG2a isotype control, anti-trinitrophenol (2A3)	BioXell	Cat# BE0089; RRID: AB_1107769
Chemicals, peptides and recombinant peptides		
Recombinant mouse IL-23	Biolegend	Cat# 589004
Recombinant Human TGF-β1	R&D	Cat# 240-B-002
Fixable Viability Dye-eFluor 506	eBioscience	Cat# 65-0866-18
Fixable Viability Dye-eFluor 780	eBioscience	Cat# 65-0865-18
Fixation/Permeabilization Concentrate	eBioscience	Cat# 00-5123-43
Fixation/Permeabilization Diluent	eBioscience	Cat# 00-5223-56
Permeabilization Buffer (10X)	eBioscience	Cat# 00-8333-56
Collagenase from *Clostridium histolyticum* (Collagenase, Type IV)	Sigma-Aldrich	Cat# C5138
DNase I	Roche	Cat# 11284932001
Collagenase/Dispase	Sigma-Aldrich	Cat# 11097113001
Western Lightning® Plus-ECL, Enhanced Chemiluminescence Substrate	PerkinElmer	Cat# NEL104001EA
PMA	Sigma-Aldrich	Cat# P1585
Ionomycin calcium salt from *Streptomyces conglobatus*	Sigma-Aldrich	Cat# I0634

(*Continued on next page*)

Continued

REAGENT or RESOURCE	SOURCE	IDENTIFIER
EDTA (Ethylene diamine tetra acetic acid) disodium salt	BDH	Cat# ACS 345
RPMI 1640 Medium	GIBCO	Cat# 11875119
HBSS, calcium, magnesium	GIBCO	Cat# 24020117
DPBS, no calcium, no magnesium	GIBCO	Cat# 14190144
FBS (fetal bovine serum)	Wisent	Cat# 081-105
EvaGreen 2X qPCR mastermix without ROX	ABM	Cat# ABMMmix-S-XL
DNase/RNase-Free Distilled Water	Invitrogen	Cat# 10977015
Aquaphor Healing Ointment	Eucerin	DIN 02009609
3.75% Imiquimod (Zyclara) cream	Valeant	DIN 02340445
NEOSPORIN® Original Ointment	HeliDerm	DIN 00666122
Lucifer Yellow CH dilithium salt	Sigma-Aldrich	Cat# L0259
DAPI	Sigma-Aldrich	Cat# D9542
Acetone	Thermo Fisher	Cat# A16P-4
Paraformaldehyde solution 4% in PBS	Affymetrix	Cat# AAJ19943K2
10% Formalin	Thermo Fisher	Cat# SF100-4
Sulfuric acid solution, 1M	Honeywell Fluka	Cat# 15644920
Critical Commercial Assays		
IL-17A Mouse Uncoated ELISA Kit	Invitrogen	Cat# 88-7371-88
IL-13 Mouse Uncoated ELISA Kit	Invitrogen	Cat# 88-7137-88
IFN-γ Mouse Uncoated ELISA Kit	Invitrogen	Cat# 88-7314-88
DNeasy Blood & Tissue Kit	QIAGEN	Cat# 69506
RNeasy Mini Kit	QIAGEN	Cat# 74104
RNAscope 2.5 HD Detection Reagent - RED kit	Advanced Cell Diagnostic	Cat# 322360
Deposited Data		
Nanostring gene expression of skin tissue	This paper	https://doi.org/10.17632/kg7snhhxzm.1
Experimental Models: Organisms/Strains		
Mouse: C57BL/6 (B6)	Jackson Lab	Stock No: 000664 | Black 6
Mouse: CD109−/−	Masahide Takahashi (Japan)	PMID: 22846721
Mouse: Pep Boy, B6 Cd45.1	Jackson Lab	Stock No.002014 | B6 Cd45.1
Mouse: B6.129P2(Cg)-Rorc^{tm2Litt}/J	Jackson lab	Stock No: 007572 | Rorc(γt)-EGFP
Oligonucleotides		
See Table S1		N/A
Software and Algorithms		
FlowJo	BD	https://www.flowjo.com
GraphPad Prism 7	GraphPad Software	https://www.graphpad.com
nSolver4.0	NanoString Technologies	https://www.nanostring.com
Other		
VWR clear frozen section compound	VWR	Cat# 95057-838
ProLong diamond antifade mountant	Invitrogen	Cat# P36961

LEAD CONTACT AND MATERIALS AVAILABILITY

This study did not generate new, unique reagents. However, further information and requests for resources, protocols and reagents described herein should be directed to and will be fulfilled by the Lead Contact, Irah King (irah.king@mcgill.ca).

EXPERIMENTAL MODEL AND SUBJECT DETAILS

CD109$^{+/+}$, *CD109*$^{+/-}$, *CD109*$^{-/-}$, CD45.1+, Rorγt$^{GFP/+}$ and Rorγt$^{GFP/GFP}$ male and female (8-24 weeks old) on a C57BL/6 background were bred and used under specific pathogen-free conditions at the Comparative Medicine & Animal Resources Centre at McGill

University. CD109−/− mice on a C57BL/6J/129S6 background were generated by Dr. Masahide Takahashi (Nagoya University) (Mii et al., 2012). Embryos were generously provided by Dr. Takahashi and injected into 0.5 pseudopregnant CD1 females. Progeny were crossed to C57BL/6 mice at least five times before use. All experiments involving *CD109*$^{-/-}$ mice used littermates as controls or mice originally derived from *CD109*$^{+/-}$ breeders. Rorγt$^{GFP/GFP}$mice were original purchased from Jackson (stock #007572) and bred with our C57BL/6 colony. All animal studies were approved by the McGill University Animal Care Committee.

METHOD DETAILS

Immunoblots

Total protein concentration of ultrasonicated samples was assessed by protein quantification assay under the manufacturer's instructions. The lysates were then diluted in a 6 × loading buffer, and incubated at 100°C for 5 min. Next, samples were separated by SDS-PAGE and transferred on polyvinylidene difluoride membranes by wet blotting. The membrane was blocked by 5% milk powder in 1 × TBS/0.1% Tween-20 (TBST) at room temperature for 1 hour and incubated in primary antibody overnight at 4°C. Membrane was washed 3 times and incubated with secondary antibody for 1 hour at room temperature. The blots were detected by the chemiluminescence light-detecting kit.

Histology and RNA scope

For histology, skin tissue was fixed in 10% formalin, paraffin embedded, sectioned and stained with hematoxylin and eosin by the MUHC-RI Histology Core. For RNAscope, formalin-fixed paraffin-embedded skin samples were stained with RNAscope® 2.5 HD red detection reagent kit including sequence-specific probes for CD109. Stained slides were scanned at either 20 × or 40 × magnification. Slides were visualized using ImageJ software.

Isolation of skin cells

To prepare single cell suspensions from skin tissue, ears were cut across the hairline and manually partitioned into rostral and caudal sides using fine scalpels. To partition the epidermis from the dermis, each side was incubated dermal side down in separation buffer (RPMI 1640 containing 1mg/ml Collagenase/Dispase) for 1.5 hours in a 35 mm Petri dish at 37°C. The epidermis and dermis were then rinsed in cold PBS, cut into ~2mm^2 pieces and incubated with digestion buffer (RPMI 1640 containing 154 U/ml Collagenase IV, 200 U/ml Dnase I and 2% FBS) for 2 hours in 24 well plates at 37°C. For spontaneous cytokine detection by flow cytometry, the protein transport inhibitor Golgistop (BD bioscience) was added into the digestion buffer (4 μL Golgistop per 6ml buffer). Following the incubation, the tissue was pipetted up and down in the digestion buffer to generate a single cell suspension, passed through a 100 μm cell strainer and collected into a 50 mL conical tube. Any residual tissue pieces were crushed using a syringe plunger before all cell strainers were rinsed with RPMI 1640 media containing 10% FBS and 15mM HEPES. Cells were then washed and resuspended in R10 buffer prior to counting.

Flow cytometry

For extracellular staining, single cell suspensions were incubated with fixable viability dye in 100 μL PBS (eBioscience), washed and incubated with anti-Fc receptor (clone 2.4G2, BD biosciences) for 10 minutes before adding fluorochrome-labeled antibodies at predetermined concentrations in 100 μL FACs buffer (PBS containing 2% FBS and 10mM HEPES) for 30 minutes on ice. For intracellular staining, cells were incubated with fixable viability dye and fixed with the Intracellular fixation/permeabilization buffer (eBioscience) according to the manufacturer's instructions, followed by antibody labeling in 100 μL permeabilization buffer. After intracellular labeling, cells were washed and resuspended in 300 μL FACS buffer. Data were acquired on a LSR Fortessa (BD Biosciences) and then analyzed with FlowJo software.

Skin-T cell co-cultures

Single cell suspensions from total skin tissue was generated as described above and re-suspended in 5 mL R10 buffer, then pipetted onto 5 mL Ficoll at room temperature in a 50 mL Falcon tube. Tubes were centrifuged for 20 min at room temperature. Live cells were isolated from the media-Ficoll interface and washed with 45 mL R10 buffer prior to suspension in culture media. Total CD3+ T cells were isolated from the skin-draining lymph nodes using T cell isolation kit (STEMCELL Technologies). 5 × 10^5 live skin cells and 1 × 10^6 T cells were mixed and added into a 24-well plate and cultured for 24 hours in various conditions. Anti-IL-23p19 antibodies (G23-8, BioXcell) or Rat IgG1 isotype control were added to some wells. Culture supernatants were collected and processed for IL-17A detection by ELISA (Invitrogen).

Tissue processing and confocal microscopy

In brief, ear samples were embedded and flash frozen in OCT, cut into 6-8 μm sections and fixed on superfrost slides with ice-cold fixation solution (75% Acetone+25% Ethanol), blocked by anti-Fc receptor for 1 hour, stained with fluorochrome-conjugated antibodies cocktail for 1 hour and nuclei staining (DRAQ5, eBiosciences) for 5 minutes at room temperature. For whole-mount staining, mouse ears were depilated with Nair and transferred into the fixation solution for 20 minutes at room temperature. For epidermal whole-mount staining, mouse tail skin (~1cm^2) was depilated with Nair followed by a digestion in 5mM EDTA for 4 hours at 37°C

to separate the epidermis. Then the epidermis sheets were transferred into 4% Paraformaldehyde for 1 hour. Following fixation, tissue was incubated in PBS containing 25U of Collagenase IV at 37°C for 30 minutes prior to antibody labeling as described above.

Quantitative RT-PCR analyses

Ear skin from individual animals were separated into epidermal and dermal sheets as described above. Samples were flash frozen and total RNA was extracted by using the QIAGEN RNeasy Mini Kit as per the manufacturer's instructions. Next, equal amounts of RNA from each sample were reverse-transcribed by QuantiTect Reverse Transcription Kit (Thermofisher). Primers (*Ccl20, Il17, Ifng, Il4, Il5, Il13, Il23a, Il12a, IL12b, S100a7, S100A8, S100A9, RegIIIg* and *Cramp*) were designed specific for the target genes and tested by end-point PCR first. Relative expression of genes of interest was measured by real-time RT-PCR. The expression of the genes of interest from individual cDNA samples were normalized to the reference gene *Hprt* and expressed as a fold change using the $^{\Delta\Delta}$Ct formula.

Nanostring analysis

Samples were divided into 4 groups (epidermis_KO, epidermis_WT, dermis_KO and dermis_WT) and were analyzed in biological triplicates. Total RNA was isolated from the epidermis and dermis of *CD109*$^{+/+}$ and *CD109*$^{-/-}$ ears and the gene expression profile is determined using a Nanostring codeset. Data were analyzed with nSolver® 4.0 software. Internal positive controls and housekeeping gene controls were selected by the nCounter Expression Data Analysis Guide. The geometric mean of internal postive controls and housekeeping genes were used to normalize the sample gene expression and variability control correspondingly. Normalized sample genes were analyzed and ranked by the magnitude of alteration. For pathway analysis, data were analyzed according to the nSolver® software advanced analysis tools.

Anti-IL-12/23p40 administration

Mice were intraperitoneally injected with 200 μg anti-IL-12/23p40 antibody (C17.8) or isotype IgG2a (2A3) purchased from BioXCell every third day for two weeks. Frequency and number of IL-17-producing γδT cells from epidermis and dermis were detected by flow cytometric analysis.

Imiquimod-induced skin inflammation

Dorsal ears of 8-10 wk old mice were treated with 3-4mg 3.75% IMQ cream (Zyclara) for 7 consecutive days. Control mice were left untreated. Ear thickness was measured by a digital Vernier caliper (accuracy: 0.01mm, Proster).

Topical antibiotic treatment and 16S rRNA quantification

Neosporin® or the vehicle control Aquaphor was applied to the dorsal and ventral ear skin of mice daily for one week using a sterile microspoon.

ELISA

Cell supernatants were collected and tested for mouse IL-17A, IFN-γ and IL-13 mouse ELISA kit (Invitrogen) as per the manufacturer's instructions.

Bone marrow chimera generation

8-10 week old WT or *CD109*$^{-/-}$ mice were irradiated with 900 rads and subsequently i.v injected with 5 × 10^6 adult bone marrow cells and, in some cases, supplemented with 1 × 10^6 neonatal thymocytes from 2-3 day old mice simultaneously. Donor and recipient cells were distinguished by CD45 alleles: WT (CD45.1)→WT (CD45.2), WT (CD45.1)→KO (CD45.2), and KO (CD45.2)→WT (CD45.1). After 12 weeks reconstitution, mice were sacrificed for flow cytometric analysis.

Percutaneous absorption studies

Sections of back skin (3 cm^2) from neonatal (postnatal day 1) or adult (> 8 weeks old) was depilated and hypodermis was gently removed by scraping with a scalpel. Skin sections were placed over a 5 mL beaker containing 5 mL PBS (dermis down, exposed to the liquid surface). 200 μL of 1mM Lucifer yellow (452 Da, Invitrogen) was added onto the epidermis and incubated at 37°C, 5% CO2. At 2 or 4 hours post-incubation, the optical density of the underlying saline solution was read using a spectrophotometer (Infinite M1000, Tecan) with excitation and emission wavelengths at 425 and 550 nm, respectively.

16S rRNA sequencing of skin microbiota

Six and twelve week-old *CD109*$^{+/+}$ and *CD109*$^{-/-}$ littermates were used for microbiome analysis. Back skin was shaved with hair clippers and cleaned with a Kimwipe. Under a sterile biosafety cabinet, FLOQSwabs from Copan Diagnostics were moistened with sterile PBS and firmly swabbed over the shaved back skin of each mouse for four minutes using a rotating movement. The tips of the swabs were cut and immediately placed in an Eppendorf tube containing 1ml of sterile PBS and frozen at −80°C for later analysis. Moistened swabs exposed to ambient air were used as negative controls. DNA was extracted from thawed swabs using the QIAGEN QIAamp DNA Microbiome Kit and quantified using the Picogreen assay. Frozen DNA samples were sent to The Children's

Hospital of Philadelphia Microbiome Center for sequencing. The V1 to V3 hypervariable regions of the 16S ribosomal DNA segment was amplified using primers specific to this region. Each amplicon was sequenced and the sequencing data was processed and analyzed using the QIIME2 pipeline as described in [https://peerj.com/preprints/27295]. Samples containing less than 5,000 reads (including two negative control samples) were excluded from further analysis. DADA2, implemented as a QIIME2 plug-in, was used for sequence quality filtering (Callahan et al., 2016). Taxonomic analysis was done using a Naive Bayes classifier trained on the Greengenes 13_8 99% OTUs. For diversity metrics including the Faith phylogenetic diversity and UniFrac distances, a rooted phylogenetic tree was generated: first, a multiple sequence alignment was performed using MAFFT (Katoh and Standley, 2013) and high variable positions were masked to reduce noise in a resulting phylogenetic tree. A mid-point rooted tree was then generated using FastTree (Price et al., 2010). Statistical analyses were carried out using R (version 3.6.0). Shannon index and richness were calculated using the package vegan (version 2.5-5). Plots were generated using the package ggplot2 (version 3.1.1).

QUANTIFICATION AND STATISTICAL ANALYSIS

Data were analyzed with Graphpad® Prism 7. Unpaired Student's t test or Two-way ANOVA followed by Sidak's multiple comparisons test were used as appropriate. *$p < 0.05$, **$p < 0.01$, ***$p < 0.001$ and ****$p < 0.0001$.

DATA AND CODE AVAILABILITY

The Nanostring dataset supporting the current study has been deposited at https://data.mendeley.com and can be accessed using the following https://doi.org/10.17632/kg7snhhxzm.1